The role of Imp and Syp RBPs in precise neuronal elimination by apoptosis through the regulation of TFs

Wenyue Guan, Ziyan Nie, Anne Laurencon, Mathilde Bouchet, Christophe Godin, Chérif Kabir, Aurélien Darnas, Jonathan Enriquez

The role of Imp and Syp RBPs in precise neuronal elimination by apoptosis through the regulation of TFs

Wenyue Guan[1†], Ziyan Nie[1†], Anne Laurençon[1], Mathilde Bouchet[1], Christophe Godin[3], Chérif Kabir[1], Aurélien Darnas[1] and Jonathan Enriquez[1, 2*]

[1] Institut de Génomique Fonctionnelle de Lyon, ENS de Lyon, CNRS, Univ Lyon 1, 46 Allée d'Italie,

[2] Lead Contact

[3] Laboratoire Reproduction et Développement des Plantes, Univ Lyon, ENS de Lyon, UCB Lyon 1, CNRS, INRA, Lyon, France

[†] These authors contributed equally

*Correspondence: jonathan.enriquez@ens-lyon.fr (J.E.)

SUMMARY

Neuronal stem cells generate a limited and consistent number of neuronal progenies, each possessing distinct morphologies and functions. These two parameters, involving the precise production of neurons with distinct identities, must be meticulously regulated throughout development to ensure optimal brain function. In our study, we focused on a neuroblast lineage in *Drosophila* known as Lin A/15, which gives rise to motoneurons (MNs) and glia. Interestingly, Lin A/15 neuroblast dedicates 40% of its time to producing immature MNs that are subsequently eliminated through apoptosis. Two RNA-binding proteins, Imp and Syp, play crucial roles in this process of neuronal elimination. We found that Imp+ MNs survive, while Imp-, Syp+ MNs undergo apoptosis. Our results indicate that Imp promotes survival, whereas Syp promotes cell death in immature MNs. Furthermore, our investigations revealed that late-born motoneurons face elimination due to their failure to express a functional code of transcription factors (mTFs) that control their morphological fate

Late-born MNs possess a unique and distinct set of TFs compared to early-born MNs. By manipulating the expression of Imp and Syp in late-born motoneurons, we observed a shift in the TF code of late MNs towards that of early-born MNs, resulting in their survival. Additionally, introducing the TF code of early MNs into late-born MNs also promoted their survival. These findings demonstrate that the differential expression of Imp and Syp in immature MNs establishes a connection between generating a precise number of MNs and producing MNs with distinct identities through the regulation of mTFs.

Importantly, both Imp and Syp are conserved in vertebrates, suggesting that they play a central role in determining the number of neurons produced during development. The *Drosophila* model, along with its genetic tools, provides a unique opportunity to further explore and decipher the functions of these RNA-binding proteins in neural stem cells versus immature neurons. The insights gained from these studies could shed light on the broader mechanisms of neurogenesis and neuronal identity determination in more complex organisms.

INTRODUCTION

The central nervous system (CNS) receives information from the periphery, records and processes it to control different types of behavior such as communication or locomotion. This complex system relies on a network of neurons and glial cells, primarily generated during development by neuronal stem cells, to fulfill these functions. Each neuronal stem cell produces a specific number of neurons and glia with diverse identities at the appropriate time and location. The precise regulation of this process is essential, as any disruption in the molecular machinery controlling it can result in severe brain disorders or cancers. Notably, alterations in adult neurogenesis in humans can contribute to psychiatric disorders such as schizophrenia (*1*, *2*) and autism (*3*, *4*) or neurodegenerative diseases such as Alzheimer (*5*). Disruptions in neurodevelopmental programs are often observed in brain tumors, and tumors that arise in early childhood may be attributed to a dysregulation in the molecular machinery governing the termination of neurogenesis (*6*). Elucidating the precise mechanisms that regulate the appropriate number of neuronal and glial cells is not only crucial for understanding biological system development and the origins of human diseases, but also for unraveling the evolution of the central nervous system's architecture and function. Recent studies in insects have indicated that variations in the number of neurons contribute to changes in neuronal circuits and behaviors (*7*, *8*). In our research using *Drosophila*, we have identified a novel mechanism involved in controlling the accurate production of neurons during development.

In *Drosophila*, adult neurons and glia are mostly produced during larval and pupal stages by stem cells called Neuroblast (NB). Similar to vertebrates, NBs undergo asymmetric divisions to self-renew and generate neuronal and glial progenies either directly or indirectly. In *Drosophila*, two major types of NBs are responsible for producing the majority of adult neurons and glia (*9*, *10*). Type I NBs generate ganglion mother cells (GMCs) that divide once to produce neurons and glia (*11*, *12*) while type II neuroblasts generate intermediate neuronal progenitors (INPs) that undergo multiple divisions to generate glia and/or neurons(*10*, *13*, *14*). Under normal conditions, each NB in *Drosophila* produces a consistent number of mature neurons, although this number can vary between different NBs. The precise generation of a stereotypical number of progenies depends on three key parameters: the speed of NB division, the timing of NB neurogenesis termination, and programmed cell death (PCD) during the asymmetric division of GMCs. Various molecular mechanisms have been identified to regulate these parameters.

Most Type I and II NBs end neurogenesis during the early pupal stages either by accumulating the transcription factor Prospero, triggering symmetrical division and resulting in two postmitotic cells (*15*, *16*) or through a combination of autophagy and programmed cell death (*17*, *18*). Prior to the termination of neurogenesis, all NBs experience a decrease in size (*15*, *16*). The reduction in size of NBs ending neurogenesis early in pupal stages is linked to a metabolic switch that enhances oxidative phosphorylation, leading to a terminal differentiation division (*15*). Conversely, the decrease in size observed in NBs terminating neurogenesis later, such as mushroom body NBs, correlates with a reduction in the activity of phosphatidylinositol 3-Kinase (PI3K), which acts as an autophagy inhibitor (*15*, *17*). The termination of NB neurogenesis through autophagic cell death or terminal differentiation is referred to as decommissioning. The process of terminating NB neurogenesis through autophagic cell death or terminal differentiation is commonly referred to as decommissioning. The temporal control of decommissioning is influenced by extrinsic signals like the steroid hormone ecdysone (*15*, *17*) and as well as an intrinsic program characterized by the sequential expression of temporal RNA binding proteins (RBPs) such as Imp (IGF-II mRNA binding proteins) and Syp (Syncrip) expressed in opposite temporal gradients within the NB, or through a temporal cascade of transcription factors. For instance, mushroom body NBs decommission during the late pupal stage due to a prolonged expression of Imp

compared to other NBs (*19*). In the ventral nerve cord (VNC, analogous to our spinal cord), the timing of NB decommissioning is determined by temporal transcription factors, leading to apoptosis in type II NBs or terminal division in Type 1 NBs (*16*). Lastly, the decommissioning of NBs is also spatially regulated by spatial selectors such as Hox genes. For example, NB5-6 in thoracic segments produces a greater number of neurons compared to NB5-6 in the abdomen, due to the absence of abdominal hox genes (*20*).

The rate of neuroblast (NB) division is a molecularly controlled parameter that can influence the number of cells generated by a lineage. On average, NB divisions in larvae occur at a speed of approximately 80-90 minutes per division. However, this speed varies among different NBs (*21*). The heterogeneity in NB division speed appears to be regulated by the opposing temporal gradients of Imp and Syp within the NB. Imp promotes high-speed division by stabilizing *myc* RNA and increasing Myc protein levels, while Syp has an inhibitory effect on NB division speed by directly inhibiting Imp as development progresses (*22*).

Furthermore, programmed cell death (PCD) after asymmetric division of the GMC acts as another influential factor in shaping the final clonal size of each lineage. Between 40% and 50% of hemi-lineages derived from type I NBs undergo PCD (Kumar et al., 2009; Truman et al., 2010). Interestingly, when PCD is blocked in the midline NBs of the VNC, the "undead" neurons differentiate and form complex and functional arborizations (Pop et al., 2020). Recent studies have demonstrated how variation in PCD patterns between different insect species could change their behavior suggesting that probably all mechanisms controlling the number of neurons potentially play a role during the behavior evolution (Pop et al., 2020; Prieto-Godino et al., 2020).

The diverse characteristics of neural stem cells (NBs), such as their proliferation termination, proliferation rate, and the generation of a GMC producing a dying cells by asymmetric division, may account for the varying number of neurons produced by individual NBs. Here, we have discovered that the fate of immature neurons also plays a crucial role in shaping the final number of neurons produced by a single stem cell.

In this study, we investigated a specific *Drosophila* lineage known as Lin A (also called Lin 15), which gives rise to 29 adult motoneurons (MNs) per ganglion, responsible for innervating leg muscles during the adult stage. This lineage also produces most of the astrocytes and ensheathing glia of the thoracic ganglion (*23–25*) **(Fig. 1A-B4)**. The process of division in Lin A/15 NB during larval stages follows a particular pattern termed type Ib **(Fig. 1C-G)**. Initially, Lin A/15 NB generates intermediate mother cells (IMCs) that give rise to a postmitotic cell and a proliferative glioblast **(Fig. 1G)**. Subsequently, during a second phase, Lin A/15 switches to a classical type I division mode, producing only postmitotic MNs **(Fig. 1G)** (*25*). As development progresses, an adult Lin A/15 consists of a predetermined number of MNs **(Fig. 1F)**. Interestingly, during larval stages, Lin A/15 NB produces an excess of neurons, which are selectively eliminated before reaching the adult stage **(Fig. 1F)**.

We first established that after producing glia and MNs, Lin A/15 GMCs produce one postmitotic MN and a sibling cell that is eliminated by PCD shortly after birth. This mode of division continues until the decommissioning of Lin A/15 NB by PCD, resulting in the production of supernumerary MNs. The excess MNs are then precisely and progressively eliminated by PCD from early pupal stages until the end of Lin A/15 neurogenesis, eventually reaching the final number of 29 MNs. Both the decommissioned Lin A/15 NB and the MNs eliminated by PCD are characterized by being Imp- and Syp+.Through genetic manipulations, we discovered that altering the temporal and spatial expression patterns of Imp and Syp in immature MNs can change the timing of NB decommissioning and the number of immature MNs that survive. Further analysis of the expression patterns of various transcription factors (TFs) published on our previous work (*26*), using the computational tool PCCD 2.0, revealed that the last-born MNs exhibit a distinct set of TFs compared

to the first-born MNs. Moreover, we found that changes in the expression levels of Imp and Syp directly affect the expression of at least three TFs (Nvy, Jim, and RunXA). Overexpression of Imp induces Jim expression and downregulates RunXA and Nvy in the last-born surviving MNs. This regulation of TF codes by Imp and Syp occurs at least in MNs 29 to 34. Notably, the new set of TFs induced in the last-born MNs closely resembles the TF code seen in earlier-born MNs (MNs 16 to 24). To further validate our findings, we artificially imposed a code found in young MNs onto the surviving last-born MNs by overexpressing Jim and suppressing Nvy function. This manipulation resulted in the survival of the last-born MNs. These results suggest that the last-born MNs undergo apoptosis due to their failure to express a functional TF code, and this code is post-transcriptionally regulated by the opposite expression of Imp and Syp in immature MNs.

Previous studies and our work cements the role of Imp and Syp as two multitasking proteins that can modulate the number of neuronal cells through different mechanisms: the timing NB decommissioning (*19*) and NB division speed (*22*) and the number of MNs surviving (this work).

RESULTS

Lin A/15 switches to a classical type I division during larval stages where the GMC produces one MN and a dying cell.

Lin A/15 produces MNs and glia during the first phase of NB division and only MNs during a second phase. It has been suggested that during the second phase Lin A/15 GMCs could produce a MN and an apoptotic sibling cell (*27*).

We precisely characterized Lin A/15 development by labeling it with GFP during the first and the second phase of NB division by using a Lin A/15 tracing system (*28*, *29*) and immuno-stained it against a cleaved form of the *Drosophila* caspase-1 (cDcp1), an apoptotic marker **(Fig. 2)**. During the first phase, 40-49 hours After larval hatching (ALH), no cDcp1+ cells were observed, confirming our previous study that during early developmental stages Lin A/15 NB produces an intermediate mother cell (IMC) that divides once to produce a glioblast and a postmitotic MN **(Fig. 2A1-A3)** (*25*). During the second phase, 53-96 hours AHL, apoptotic cells cDcp1+ Elav- were detected close to Dpn+ Lin A/15 NB (Dpn and Elav are NB and postmitotic neuronal markers respectively), suggesting that PCD occurs soon after asymmetric division. The absence of Elav in the apoptotic cells also suggested that the sibling cells die before acquiring a neuronal identity **(Fig. 2B1-F3)**. Consistent with this idea, we then generated Lin A/15 MARCM clones to label all Lin A/15 cells with GFP under the control of a *tub-Gal4* transgene, and *VGlut*+ MNs with mCherry by using *VGlut-LexA::GAD*, a gene trap transgene of the gene coding for the vesicular glutamate transporter expressed by all *Drosophila* MNs. We dissected late third instar larva (LL3) and observed that cDcp1+ Elav- cells did not express *VGlut* **(Fig. 2G1-G3)**.

Together, our results show that Lin A/15 GMCs produce a MN and a sibling cell eliminated by PCD during the second phase of Lin A division **(Fig. 2H)**. Moreover, PCD of the sibling cell occurs soon after birth before they express neuronal marker such as Elav or *VGlut*.

Lin A/15 NB decommissions 24h after pupa formation through PCD

We subsequently explored the development of Lin A/15 during the pupal stages to determine when the NB stops producing MNs and terminates neurogenesis.

We genetically labeled Lin A/15 with GFP and performed an immunostaining against Dpn to label Lin A/15 NB and against phospho-Histone H3 (PH3), a marker of cell proliferation. We revealed that Lin A/15 NB (PH3+/Dpn+) continues proliferating from 0 hour after pupa formation (APF) until 20 hours APF **(Fig. 3A1-C3)**. During early pupal stages cDcp1+ Elav- cells were also detected suggesting that Lin A/15 NB keep producing a GMC that divides once into a MN and an apoptotic cell **(Fig. S1)**. At 24 hours APF, Lin A/15 NB is no longer detected in most of our samples (N=4/17,

Number of Lin A/15 with a NB), revealing the end of Lin A/15 neurogenesis at this stage. Similar to what has been shown for other NBs, the volume of Lin A/15 NB decreases throughout development until the termination of Lin A/15 neurogenesis **(Fig. S2)**. At 24 hours APF, the remaining Lin A/15 NBs are extremely small and express cDcp1 suggesting a decommissioning of Lin A/15 NB through PCD **(Fig. 3D)**. To confirm this result we then inhibited PCD in Lin A/15 by using the baculovirus P35 protein, an inhibitor of apoptosis in insect (*30*). Under these experimental conditions, Lin A/15 NB survived at least until 28 APF **(Fig. 3E-G)**. Furthermore we didn't detect autophagic markers in the NB such as Atg8 and LysoTracker (*31*) suggesting that the PCD of the NB is not linked to autophagy such as the mushroom body NBs **(Fig. S3).**

Our results reveal that Lin A/15 NB continues producing MNs during early pupal stages and, unlike most NBs described in the thoracic segments of the VNC (*16*), Lin A/15 NB terminates its proliferative phase through PCD at 24 hours APF in all thoracic ganglions **(Fig. 3H)**.

Opposite temporal gradients of Imp and Syp control the timing of Lin A/15 NB decommissioning

We conducted further investigations to determine whether Imp and Syp could regulate the timing of decommissioning of Lin A/15 NB.

During Lin A/15 neurogenesis, we carefully examined the expression pattern of Imp and Syp in Lin A/15 NB. At early L3 stages, Imp is highly expressed in Lin A/15 NB, while Syp protein is not detectable (46-56 hours ALH) **(Fig. 4A1-A2, F1-F2)**. As neurogenesis progresses, Lin A/15 NB starts expressing Syp at mid-L3 larval stages, while the expression of Imp begins to decrease (70-73 hours ALH) **(Fig. 4B1-B2, G1-G2)**. Towards the end of the larval stages, there is a reversal in the expression pattern of Imp and Syp in Lin A/15 NB, with Imp being weakly expressed and Syp being highly expressed **(Fig. 4C1-C2, H1-H2)**. This opposite expression of Imp and Syp becomes more pronounced during pupal stages, where Imp protein is no longer detectable in the NB just before decommissioning **(Fig. 4D1-E2, I1-J2).**

To investigate the impact of Imp and Syp on the lifespan of Lin A/15 NB, we conducted specific manipulations. Knocking down Imp in Lin A/15 NB resulted in premature decommissioning at 20 hours APF **(Fig. 5A1-G)**. Conversely, prolonging the expression of Imp or knocking down Syp led to an extension of Lin A/15 NB's lifespan until the young adult stages and at least 28 hours after pupa formation (APF), respectively **(Fig. 6A1-J)**. Furthermore, we observed that the temporal expression of Imp/Syp controls the timing of Lin A/15 NB decommissioning similarly in all thoracic segments. Additionally, we generated Syp overexpression (OE) MARCM clones, and interestingly, we did not observe any significant effect on the number of MNs produced in adult flies **(Fig. S4)**. As a result, we decided not to delve further into Syp function in this particular genetic background.

Our findings provide evidence that the sequential expression of Imp and Syp plays a crucial role in regulating the timing of Lin A/15 NB decommissioning, ultimately terminating neurogenesis through apoptosis in all thoracic segments **(Fig. 4K)**.

The last-born neurons produced by Lin A/15 are eliminated by PCD.

The number of Lin A/15 motoneurons (MNs) in adult flies is highly consistent and gradually established during development **(Fig. 1F and Fig. 7K)**. At 0 hour APF, Lin A/15 reaches its maximum number of Elav+ neurons (N=39, SD=2, Number of Lin A/15 Elav+ neurons) **(Fig. 7K)**. However, even though Lin A/15 NB continues to divide in early pupal stages **(Fig. 3A-3C)**, the number of Elav+ neurons progressively decreases until reaching almost the final number of MNs at 24 hours APF (N=32, SD=1 at 24 hours APF compared to adult: N=29, SD=1) (**Fig. 7K**).

To investigate if the supernumerary postmitotic MNs are eliminated by programmed cell death (PCD), we genetically labeled Lin A/15 with GFP and performed immunostaining against Dpn, Elav,

and cDcp1 during pupal stages **(Fig. 7A1-C3)**. Unlike in larval stages, we detected Elav+ cDcp1+ neurons close to the NB, indicating that the last-born Elav+ neurons are progressively eliminated by apoptosis from 0 hours to 24 hours APF **(Fig. 7A1-C3)**. To further confirm that the last-born MNs are eliminated by PCD, we fed L3 larvae with Edu to label only the late-born MNs and dissected the central nervous system (CNS) at early pupal stage (5 hours APF) **(Fig. 7D1-D7)**. The first-born MNs were Edu- (N=30, SD=2, Number of Edu- MNs at 5 hours APF) and located away from the NB, while the last-born MNs (N=7, SD=2, Number of Edu+ MNs at 5 hours APF) were Edu+ and positioned close to the NB **(Fig. 7 D5-D7)**. Additionally, we found that cDcp1+ Elav+ neurons were always Edu+, and no cDcp1+ Edu- neurons were observed (N=16, Number of Lin A/15 analyzed). Further dissection of CNSs at late pupal stage (17 hours APF) showed a significant decrease in the number of Elav+ Edu+ MNs (N=2, SD=2, Number of Edu+ MNs at 17 hours APF), confirming the progressive elimination of all these late-born MNs **(Fig. 7D1-F)**. Both results indicate that the last-born MNs undergo PCD during pupal stages.

To confirm that the supernumerary MNs are eliminated by programmed cell death (PCD), we conducted an experiment to inhibit apoptosis in MNs by ectopically expressing the antiapoptotic gene P35. For this purpose, we employed the MARCM technique with the *VGlut-Gal4* (also known as OK371-Gal4) enhancer trap driver to express P35 specifically in the supernumerary immature neurons. It's important to note that this driver is exclusively expressed in Lin A/15 Elav+ cells **(Fig. 2)**. Consequently, the expression of VGlut>P35 is expected to fail in inhibiting apoptosis in the Elav- cells eliminated by PCD after the GMC division. However, it should effectively inhibit apoptosis in the last-born Elav+ MNs during the pupal stage. As anticipated with this genetic manipulation, we observed similar numbers of neurons produced in L3 larvae in the Lin A/15 MARCM clone expressing P35 compared to the WT Lin A/15, while more Lin A MNs survived into adulthood **(Fig. 7F-J)**. These results provide further evidence supporting the notion that supernumerary MNs are indeed eliminated by PCD.

Overall, our results provide strong evidence that the elimination of supernumerary MNs by PCD is not random. Instead, only the last-born neurons are precisely and progressively eliminated through PCD during pupal stages from 0 hour APF to 24 hours APF **(Fig. 7L)**.

Opposite spatial gradients of Imp and Syp in postmitotic Neurons determine the pattern of PCD

The serially derived neuronal progenies inherit the levels of Imp and Syp from the neural stem cell (NB), resulting in the formation of opposite spatial gradients of Imp and Syp in postmitotic MNs (Imp is highly abundant in first-born MNs, while Syp is highly present in late-born MNs) **(Fig. 4A-J)**. In our previous studies we have shown that during larval stages *Imp* and *Syp* are also actively transcribed in postmitotic MNs.

Notably, during pupal stages, the last-born Lin A/15 MNs that are eliminated by programmed cell death (PCD) are Imp- and Syp+ **(Fig. 8A1-A5)**. These observations suggest that the distinct expression patterns of these two RNA-binding proteins (RBPs) in postmitotic neurons may play a crucial role in determining the final number of adult MNs surviving. Consequently, we sought to explore the possibility that Imp and Syp not only control the size of a lineage through their temporal function in the NB **(Fig. 5)** but also by regulating PCD in postmitotic neurons.

Our genetic tools not only enable us to study the decommissioning of Lin A/15 NB under various genetic conditions but also to precisely investigate the fate of its progeny. Knocking down Imp in Lin A/15 resulted in premature PCD of Elav+ MNs during larval stages **(Fig. 8C1-D3)** and an increase in the number of Elav+ neurons eliminated by PCD during pupal stages **(Fig. 8B1).** Conversely, By prolonging the expression of Imp or knocking down Syp in Lin A/15 NB and its progeny, we were able to inhibit PCD of the supernumerary neurons **(Fig. 8B2, 8E1-J3)**. These genetic experiments, which manipulated the levels of Imp and Syp in the NB and its postmitotic

progeny, led to changes in the final number of neurons produced by Lin A/15 **(Fig. 8K)** by altering the timing of NB decommissioning and the pattern of PCD in postmitotic neurons **(Fig. 7-8)**. The modulation of PCD pattern in postmitotic neurons by Imp and Syp could result from an autonomous function in postmitotic MNs or a change in the temporal identity of Lin A/15 NB. To separate their functions in the NB and MNs, we ectopically expressed Imp in postmitotic neurons, including the supernumerary MNs, without affecting its expression in Lin A/15 NB, using the MARCM technique with the *VGlut-Gal4* enhancer trap driver. Under this experimental condition, more Lin A MNs were maintained in adult flies **(Fig 8L1-N)**, implying a cell-autonomous function of Imp in promoting cell survival of MNs.

In conclusion, our findings demonstrate that the opposite expression pattern of Imp and Syp in postmitotic neurons precisely shapes the size of Lin A/15 lineage by controlling the pattern of PCD in immature MNs **(Fig. 8)**.

The last-born MNs that are eliminated by PCD are primed with a specific combination of TFs under the control of Imp and Syp.

In our previous study, we demonstrated that the first 29 MNs express a specific set of mTFs that determine the target muscle of each MN. Furthermore, we revealed that at least 5 out of the 16 TFs expressed in these first 29 MNs are post-transcriptionally regulated by the opposite gradients of Imp and Syp. Based on these findings, we hypothesized that the precise elimination of MNs could also result from a post-transcriptional regulation of TFs by Imp and Syp.

To investigate this, we analyzed the expression of Nvy and RunXA, two transcription factors known to be expressed in last-born surviving MNs, and Jim, a TF expressed in younger MNs in LL3, just before the elimination of the last-born MNs. To achieve this, we utilized a new version of our computational tool (PCCD V2.0), which allows for a more precise determination of the TF code in last-born MNs (see material and methods). Our results revealed that last-born MNs express a specific combination of TFs, with high levels of Nvy and RunXA and no expression of Jim **(Fig 9A, E, I, and M)**. Next, we manipulated the expression levels of Imp and Syp in Lin A/15.

By overexpressing Imp or knocking down Syp in Lin A/15 neural progenitors and their progeny, the number of Jim+ MNs increased from 8 to 15 and 14 MNs, respectively **(Fig 9A1-A3, B1-B3, C1-C3)**. PCCD analysis demonstrated that last-born MNs express Jim de novo when Imp is overexpressed or Syp is knocked down **(Fig 9A4, B4, C4, and M)**.

RunXA is expressed in two cluster of MNs in young and in last born MNs with high level of expression in the MNs eliminated by PCD during the pupal Stages **(Fig 9 E1-E4 and M)**. The overexpression of Imp or the knowing down of Syp reduce drastically the number RunXA+ MNs **(Fig 9 F1-F3, G1-G3, H1-H2)**. The PCCD method reveals that the expression is completely abolished in last born MNs while it it not affected in the youngest cluster of MNs when Imp is overexpressed or Syp knocked down **(Fig. F4, G4 and M)**.

Nvy shows a similar expression pattern compared to RunXA **(Fig 9I1-I4 and M)**. The overexpression of Imp or the knockdown of Syp slightly reduces the number of Nvy+ MNs from 16 to 11 MNs **(Fig 9J1-L2)**. PCCD analysis shows that the number of MNs expressing Nvy is only reduced in the last-born cluster of MNs when Imp is overexpressed or Syp is knocked down, while it is not affected in the youngest cluster of MNs **(Fig 9J4, K4, and M)**. Importantly, even though the expression of Nvy is not completely abolished in last born MNs like RunXA, its expression is drastically reduced compared to control Lin A/15 **(Figure I2, J2, and K2)**.

Overall, these results demonstrate that overexpressing Imp or knocking down Syp changes the combination of TFs in last-born MNs from Nvy ^{high}, RunX ^{high}, and Jim^{-} to Nvy ^{low}, RunXA^{-}, and Jim^{+}.

Changing the combination of TF in last-born MNs leads to MNs survival.

Overexpressing Imp or knocking down Syp leads to the expression of a TF code in last-born MNs resembling the code found in earlier MNs (MNs 16 to 23), characterized by Nvy-, RunXA-, and Jim+. These findings suggest that the two RNA-binding proteins, Imp and Syp, may control the number of surviving MNs through TF regulation.

To further investigate this possibility, we used the MARCM technique to change the TF code of last-born MNs without affecting the expression of Imp and Syp. In our genetic background, control MARCM clones typically produce around 26 MNs instead of 28 **(Fig10. A1-A2, E)**. We observed that in different genetic backgrounds, Lin A/15 sometimes produces fewer than 28 MNs.

When we overexpressed Jim **(Fig. 10 C1-C3)**, including in the last-born MNs, or removed Nvy **(Fig. 10 B1-B3)**, the number of MNs produced by Lin A/15 increased to approximately 32 **(Fig. E)**. Notably, in nvy-/- LinA/15 MARCM clones overexpressing Jim **(Fig. 10 D1-D3)**, the number of MNs produced is close to 50 **(Fig. 10 E)**.

These results demonstrate that imposing a TF code in last-born MNs resembling the code found in early-born MNs enables their survival until the adult stage. This suggests that the specific combination of TFs controlled by Imp and Syp plays a crucial role in determining the fate and survival of motor neurons during development.

DISCUSSION

Imp and Syp, lineage size ruler

The timing of neurogenesis termination plays a crucial role in determining the number of neurons produced during development by stem cells. Our genetic tool, which traces a single lineage, allowed us to demonstrate that altering the timing of neural stem cell decommissioning results in changes to the number of neurons generated from that stem cell. In our study, we found that two intrinsic temporal factors, Imp and Syp, actively participate in defining the final clonal size of a lineage by signaling the timely apoptosis of NBs. Previous research has indicated that both intrinsic mechanisms and external cues control the expression pattern of Imp and Syp in brain NBs. In some brain lineages, Imp and Syp cross-repress each other (*32*, *33*), and this cross-repression is influenced by external cues, such as the ecdysone hormone (*15*) or activins (*34*). However, in Lin A/15 NB, we observed that there is no mutual inhibition between Imp and Syp, suggesting that Imp/Syp-independent mechanism(s) regulate their sequential expression in Lin A/15 NB **(Fig. S5)**.

Furthermore, our investigation of a single neuronal lineage revealed that the spatial expression pattern of Imp and Syp in postmitotic neurons is also important in determining the lineage size through regulating PCD. The expression levels of Imp/Syp in immature MNs correlate with their temporal expression in the NB: first-born neurons express high levels of Imp, while last-born neurons express high levels of Syp. Interestingly, both Imp and Syp are actively expressed in immature MNs, indicating that their expression in immature MNs is not simply a consequence of their expression in the NB (*26*).

We question whether immature MNs maintain their Imp/Syp expression by inheriting determinants from the NB. If so, are these determinants directly influencing Imp/Syp expression, or do they give MNs the capacity to respond to external cues, such as the ecdysone hormone? Based on our hypothesis, we propose that postmitotic MNs, similar to their state in the NB, retain the ability to respond to external cues, which could explain why MNs are eliminated during early pupal stages when ecdysone is highly expressed (*35*).

Imp and Syp, highly versatile RBPs in specifying neuronal identity and lineage sizes

Imp and Syp are versatile proteins that play roles in various aspects of neuroblast (NB) development. Their sequential expression in brain NBs controls the temporal identity of the NB (*32*, *33*), the timing of NB decommissioning (*19*), and the speed of cell division (*22*). In the brain, their

opposing temporal expression in Mushroom Body NBs shapes the expression pattern of the Chinmo transcription factor, which, in turn, determines the identity of the neuronal progeny based on its concentration.

We have recently reveals that Imp/Syp not only control the morphology of Lin A/15 motor neurons (MNs) by determining the temporal identity of the neuroblast but also by shaping a combination of morphological transcription factors (mTFs) in postmitotic MNs, which subsequently control their morphologies (*26*). Additionally, Imp/Syp appear to regulate the expression of terminal selector genes. Originally defined in C. elegans, terminal selectors are transcription factors that maintain the expression of proteins crucial for neurons to function, such as neurotransmitters or neuropeptides (*36–39*). In the Mushroom Body, Imp/Syp shape the terminal molecular features fate by regulating the terminal selector Mamo (*40*). These findings reveal that Imp/Syp are multitasking proteins that act in both the NB and its progeny during neurogenesis, ensuring the reliable production of a specific number of neurons with unique identities. The data highlight that both RBPs control two parameters in postmitotic neurons: neuronal diversity and neuronal survival, and these two parameters are directly coordinated through the regulation of TFs by Imp and Syp.

The question of why an excess of MNs is produced and why neurons undergo programmed cell death (PCD) during development is a fundamental one in neurodevelopment. PCD is observed in various animal models studied in laboratories, from C. elegans to vertebrates, and several explanations have been proposed to understand why such mechanisms have been selected during evolution (*41*, *42*). The widespread occurrence of PCD during neurodevelopment leads to an intriguing hypothesis that neurons normally fated to die represent an important reservoir that can be used during evolution to explore different morphological possibilities. In this scenario, different mTF codes can be tested without affecting the axon-muscle connectome, allowing for the exploration of various combinations of mTFs until a functional combination is selected. This process may contribute to the diversification of neuronal morphologies and functions, ultimately shaping the complexity of the nervous system during evolution.

Imp/Syp proteins in development and disease.

Imp and Syp are evolutionarily conserved, both homologs are highly expressed in the developing mouse brain and play vital roles in neural development, suggesting a fundamental conservation of their function in the development of central nervous (*43–45*). For example, Imp1, one of the three mouse orthologues of Imp family, is highly expressed in young neuronal progenitors. Its temporal expression with other RBP partners changes the temporal identity of the neuronal stem cells. In particular Imp promotes the self-renewal state of neuronal stem cells while inhibiting differentiation genes (*46*).

As mentioned in the introduction, any dysregulation of the machinery controlling neuronal stem cell physiology can have dramatic consequences. For example dysregulation of the RBPs expression are a common feature of neurodegenerative diseases (*47*). Interestingly, the Imp family also plays a key role in the stem cell physiology of many other organs and several studies have revealed that the Imp family maintain the proliferative state of different type of cancers (*48–52*). The powerful genetic tools available in *Drosophila* allow us to decipher their functions in the stem cells versus postmitotic neurons which is a first step not only to better understand how the organ is built but also to decipher the genesis of cancer and neurodegenerative diseases.

EXPERIMENTAL PROCEDURES

Key resources table

REAGENT or RESOURCE	SOURCE	IDENTIFIER
Antibodies		
rabbit anti-Dcp1	Cell signaling	Cat# 9578S; RRID:AB_2721060
mouse anti-Elav	DSHB	Cat#9F8A9; RRID:AB_2314364
rat anti-Elav	DSHB	Cat#7E8A10; RRID:AB_528218
mouse anti-repo	DSHB	RRID:AB_528448
rabbit anti-PH3	Abcam	RRID:AB_2164915
guinea-pig anti-Dpn	Gift from Jim Skeath	N/A
goat anti-mouse Alexa 647	Invitrogen	Cat#A32728; RRID:AB_2633277
donkey anti-rat Alexa 647	Jackson	Cat#712-605-153; RRID:AB_2340694
goat anti-mouse Alexa 555	Invitrogen	Cat#A32727; RRID:AB_2633276
goat anti-rabbit Alexa 555	Invitrogen	Cat#A32732; RRID:AB_2633281
goat anti-Rat Alexa 555	Abcam	Cat#ab150166
donkey anti-guinea-pig DyLight405	Jackson	Cat#706-475-148; RRID:AB_2340470
Chemicals, peptides, and recombinant proteins		
formaldehyde	Thermo Scientific	Cat#28908
PBS	Dutscher	Cat#X0515-500
triton	Sigma	Cat#T8787-100mL
BSA	Sigma	Cat#A7906-500 g
Vectashield mounting medium	Vector Laboratories	Cat#H1000
Critical commercial assays		
Clicl-iT EdU imaging kit	Invitrogen	Cat#C10340
Experimental models: Organisms/strains		
UAD-KD (attP2[68A4])	Awasaki et al., 2014	N/A
Dpn>KDRT-stop-KDRT>CRE (su(Hw)attP8[8E10])	Awasaki et al., 2014	N/A
act>loxP-stop-loxP>LexA::P65 (attP40[25C7])	Lactin and Truman., 2016	N/A
lexAop-myr::GFP (su(Hw)attP5[50F1])	Awasaki et al., 2014	N/A
R10c12-GAL4 (3rd chromosome, attp2)	Lactin and Truman., 2016	N/A
lexAop-Imp-RNAi (attP40[25C7])	Ren et al.,2017	N/A
lexAop-Imp-RM (attP40[25C7])	Ren et al.,2017	N/A
lexAop-Syp-RNAi (attP40[25C7])	Ren et al.,2017	N/A
tub-gal4 (3rd chromosome,79A2)	Bloomington *Drosophila* Stock Center	BDSC: 5138
DVGlut-Gal4 (2nd chromosome, 22E1)	Bloomington *Drosophila* Stock Center	BDSC: 26160
DVGlut-LexA::GAD (VGlutMI04979)	This study	N/A
UAS-P35 (2nd and 3rd chromosome)	Bloomington *Drosophila* Stock Center	BDSC: 5072; 5073
20XUAS-Imp-RM-Flag (3rd chromosome)	Liu et al., 2015	N/A
actin^FRT-stop-FRT^Gal4	Gift from Alain Garces	N/A
Recombinant DNA		
pBS-KS-attB2-SA(2)-T2A-LexA::GADfluw-Hsp70 vector	Addgene	Cat#78307
Software and algorithms		
Amira 3D software (version 6.2)	SCR_007353	https://www.fei.com/

ImageJ (version 1.48)	Schneider et al., 2012	https://imagej.nih.gov/ij/
GraphPad (Prism 8)	SCR_002798	https://www.graphpad.com/scientific-software/prism/

Fly strains

Lin A/15 NB tracing system (all Figures):
LinA/15 restrictive labeling is achieved by immortalizing Gal4 expression in Lin A/15 neuroblasts and its descendants (Awasaki et al. 2014; Lacin and Truman. 2016). The following fly strains were crossed to specifically label LinA:
10c12-GAL4 crossed with *Dpn>KDRT-stop-KDRT>CRE; act>loxP-stop-loxP>LexA::P65; lexAop-myr::GFP; UAS-KD.*

The following fly strains were used to overexpress and knockdown genes (Figure 5, 7):
Dpn>KDRT-stop-KDRT>CRE; act>loxP-stop-loxP>LexA::P65; lexAop-myr::GFP; UAS-KD crossed with *LexAop-Imp-Flag/CyO; R10c12-GAL4/TM6B* to overexpress Imp
With *LexAop-Syp-RNAi/CyO; R10c12-GAL4/TM6B* to knockdown Syp
With *LexAop-Imp-RNAi/CyO; R10c12-GAL4/TM6B* to knockdown Imp

Lin A/15 MARCM:

Genetic crosses to label with GFP all Lin A cells and with mCherry *VGlut*+ Elav+ neurons (Figure 2):
y,w, hs-Flp1.22; VGlut-LexA::GAD, FRT42D, LexAop-mCherry/Cyo;tub-GAL4/TM6B crossed to y,w, hs-Flp1.22; VGlut-Gal4, UAS-mCD8::GFP, Mhc-RFP, FRT42D, tub-Gal80/CyO; UAS-mCD8::GFP/MKRS
Genetic crosses to inhibit apoptosis in immature postmitotic neurons (Figure 6):
y,w,hs-Flp$^{1.22}$; VGlut-Gal4, UAS-mCD8::GFP, Mhc-RFP FRT42D/Cyo; TM6B/MKRS crossed to *y,w,hs-Flp$^{1.22}$; VGlut-GAL4, UAS-mCD8::GFP, Mhc-RFP, FRT42D, tub-Gal80/CyO; UAS-P35/TM6B*.

Genetic crosses to overexpress Imp only in postmitotic neurons (Figure 7) :
y,w,hs-Flp$^{1.22}$; VGlut-Gal4, UAS-mCD8::GFP, Mhc-RFP, FRT42D/Cyo; TM6B/MKRS crossed to *y,w,hs-Flp$^{1.22}$; VGlut-GAL4, UAS-mCD8::GFP, Mhc-RFP, FRT42D, tub-Gal80/CyO; UAS-Flag-Imp-RM/TM6B*.

Genetic crosses to generate *nvy-/-* and *nvy-/-* Jim overexpression Lin A clones
y, w, hs-Flp, UAS-mCD8::GFP; VGlut-Gal4, FRT42D, nvy- / CyO; 10XUAS-myr::GFP / MKRS
crossed to *y,w, hs-Flp1.22; VGlut-Gal4, UAS-mCD8::GFP, Mhc-RFP, FRT42D, tub-Gal80/CyO ; UAS-Jim CDS/TM6b*

Genetic crosses to generate Jim overexpression and Control Lin A clones

y,w, hs-Flp1.22; VGlut-Gal4, UAS-mCD8::GFP, Mhc-RFP, FRT42D / CyO; TM6B / MKRS
Crossed to
y,w, hs-Flp1.22; VGlut-Gal4, UAS-mCD8::GFP, Mhc-RFP, FRT42D, tub-Gal80/CyO; UAS-jim/ TM6B

First-instar larvae (0~12h ALH) were heat shocked at 37°C for 20 minutes to induce mosaic clones in L3 larvae and at 35°C for 15min to induce mosaic clones in adults.

***Vglut-LexA::GAD* transgenic line**

The *Vglut-LexA ::GAD* transgenic line is generated by the Trojan-mediated conversion of MIMIC (Trojan-MiMIC) technique (*53*). A *pBS-KS-attB2-SA(2)-T2A-LexA::GADfluw-Hsp70* Plasmid (addgene plasmid #78307) was injected into embryos of flies bearing intronic MiMIC inserts at *VGlut* gene (VGlutMI04979) together with phiC31 integrase on the genetic background. G0 flies were crossed with flies from the *y, w; Sp/CyO; Dr/TM3, Sb* double balancer line, and y- recombinant progeny, which had lost the y+ selection marker associated with the MiMIC insertion, were isolated. The integrase-dependent exchange of *T2A-LexA::GAD*-containing cassette produce a *LexA::GAD* driver line that having an expression pattern corresponding to that of *VGlut*.

Immunohistochemistry

Immunostaining of larval and pupal CNS
Inverted L3 larvae or open pupae were fixed in 4% paraformaldehyde in PBS for 20 minutes at room temperature and blocked in the blocking buffer for one hour. L3 larval or pupal CNS were carefully dissected in PBS and then incubated with primary antibodies overnight (>=12h) and secondary antibodies in dark for one day (>=12h) at 4°C. Fresh PBST-BSA (PBS with 0.1% Triton X-100, 1% BSA) was used for the blocking, incubation, and washing steps: five times for 20 minutes at room temperature after fixation and after primary/secondary antibodies. Larval/pupal CNS were mounted onto glass slides using Vectashield anti-fade mounting medium (Vector Labs). Slides were either imaged immediately or stored at 4°C.

Immunostaining of adult VNC
After removing the abdominal and head segments, thoraces of the flies were opened and fixed in 4% paraformaldehyde in PBS for 25 minutes at room temperature and blocked in the blocking buffer for one hour. After dissection, adult VNC were incubated with primary antibodies for one day and secondary antibodies in dark for one day at 4°C. Fresh PBST-BSA (PBS with 0.1% Triton X-100, 1% BSA) was used for the blocking, incubation, and washing steps: five times for 20 minutes at room temperature after fixation and after primary/secondary antibodies. VNC were mounted onto glass slides using Vectashield anti-fade mounting medium (Vector Labs). Slides were either imaged immediately or stored at 4°C.

Primary and secondary antibodies
The primary antibodies used in this study include: mouse anti-Elav (DSHB-9F8A9), rat anti-Elav (DSHB-7E8A10), mouse anti-Repo (DSHB- 8D12), rabbit anti-cDcp1 (CellSignaling-9578), rabbit anti-PH3 (Abcam-ab80612), guinea-pig anti-Dpn (gift from Jim skeath, Skeath et al., 2017), rat anti-Imp and rabbit anti-Syp (gifts from Chris Doe).
The secondary antibodies used in this study include: goat anti-Mouse Alexa 647 (Invitrogen-A32728), donkey anti-rat Alexa 647 (Jackson- 712-605-153), goat anti-Mouse Alexa 555 (Invitrogen-A32727), goat anti-Rabbit Alexa 555 (Invitrogen-A32732), goat anti-Rat Alexa 555 (Abcam-ab150166), donkey anti-guinea-pig DyLight405 (Jackson- 706-475-148).

Image acquisition
Multiple 0,5-µm-thick (with exceptions of 1-µm-thick for Figure6 H-K and Figure L-M) sections in the z axis (ventro-dorsal for larval/pupal CNS or adult VNC) were imaged with a Leica TCS SP8 or a Zeiss LSM 780 confocal microscope. Binary images for z stack images were generated using NIH ImageJ.

5-ethynyl-2'deoxyuridine (EdU) labelling (Figure 6)
To mark late-born MNs, mid-third-instar larvae (98h-104h ALH) were transferred from standard fly food to fly food containing 250 mM EdU. Pupae were then dissected at indicated time points. Open pupae were fixed in 4% paraformaldehyde in PBS for 20 minutes at room temperature, followed by a quick wash with PBST (PBS with 0.1% Triton X-100). Edu labeling was then detected using Clicl-iT

EdU imaging kit (Invitrogen) according to manufacturer's instructions. The immunostaining was then performed as described in the **Immunostaining** section.

Neuroblast volume
Each Lin A/15 NB was segmented in 3D in ImageJ/Fiji (*55–57*), using the LimeSeg plugin (*58*), on the GFP channel, with the following parameters: D_0~4-6, F pressure=0.01, Z_scale=6.8, Range in d0 units~4-6, Number of integration step=-1, real XY pixel size=50. The volume of each segmented cell was used to make the graph on (**Fig. S2**).

Quantification and statistical analysis
Graphs of the relative position of each LinA/15 cells were generated with Microsoft Excel. The spatial coordinates were assigned to each cell using the cell counter plug-in of NIH ImageJ software. The coordinates of each cell were normalized with Microsoft Excel in order to have the position of the Lin A NB at the origin of the plot graph. For samples without NB labeled (as in Figure6 C1 and Figure7 H3), the coordinates of each cell were then normalized to a cell located ventrally (as the cDcp1 positive cell in Figure6 C1 and Figure7 H3).

The plots of the number of Elav+ cells (Figure1F, 6D, 6G,7K, 7N), Elav+ Edu+ cells (Figure 6F) and Elav+ cDcp1 cells (Figure 7B1,7B2), as well as the graph for frequency of NB (Figure 5P and 5Q) were generated with Prism (GraphPad Software). All bar errors represent standard deviation of a minimum of 7 samples, each dot represents a single sample analyzed. Otherwise, the sample size used for each genotype is indicated on the graph or in the text and/or the figures legends. Student's *t*-test (Figure 1F,6D, 6F,6G,7B,7K and 7N) or Fisher's test (Figure 5P-Q) were performed to compare the difference in between indicated groups. Differences of $P < 0.05$ were considered significant. *$0.01 < P < 0.05$; **$0.001 < P < 0.01$; ***$0.0001 < P < 0.001$. **** $P < 0.0001$.

All schematics were made in Microsoft PowerPoint (Figure1G, Figure2H, Figure3G, Figure4K and Figure 6L).

Positive Cell Cluster Detection (PCCD) method (Fig. 2, see also PCCD note book in key resources table)

The Positive Cell Cluster Detection (PCCD) method aims to link the expression of a given TF to the birth-order of an immature MN (iMN) by using the correlation between the birth-order of iMNs and their spatial organization. In our Lin A/15 model, the EdU experiments **(Fig. 1)** reveal a good correlation between the birth order of iMNs and their spatial distance from the NB in 3rd instar larvae: young born iMNs are farther away from the NB compared to older iMNs. The final goal of this method is to predict the TF code expression pattern in each iMNs in a third instar larva.

The method followed a series of steps:

Step 1: From the imaging, assign spatial x, y, z coordinates and the expression (on/off) of a given TF to each Lin A/15 cell (N>15, Number of Lin A/15 immunostained for a given TF).
Step 2: Calculate the Euclidean distance between the NB and the x, y, z, coordinates of each iMN (relative distance).
Step 3: Order iMNs in each Lin A/15 according to their distance to NB. This presents each Lin A/15 as an ordered sequence of iMNs (this defines the x axis position where cell #1 is defined as the furthest from the NB, i.e. the oldest iMNs on average). Then calculate the frequency of expression of all TFs as a function of their rank in each ordered Lin A sequence.
Step 4: Apply a filter (Savitzky-Golay) to smooth each distribution.

Step 5: Define the position in the sequence of the positive cell cluster(s) by using a peak detection method. Determine its length (average number of cells expressing a given TF in all Lin A/15 samples analyzed). Then find the position of the positive cell cluster with this average length compatible with the smoothed TF distribution. The position and its length are represented by a horizontal line.
Step 6: Assemble all positive cell clusters for each TF on the same graph to reveal combinatorial TF code for each iMN. Convert the x' axis to a birth order axis (1 to 29) since the distance between iMN and the NB is tightly linked to their birth order. Define the coverage index at the border of all cell clusters.

More details about the method include:
Frequency histograms (Step 3): The frequency histograms of positive cells can in principle be computed in an either global or relative manner. Global means that at each position i, the observed number of positive cells Pi will be normalized by the total number N of observed sequences for this TF. Thus the frequency at rank i is defined as Pi/N. By contrast in the relative definition of frequencies, at each position i, the frequency is determined by the number of positive cells Pi divided by the number of sequences Ni for which this position has been measured, leading to a frequency at rank i defined as Pi/Ni. The relative measure avoids bias that possibly arises in the global method by considering as negative (by default) cells that are not observed in sequences that are too short to reach this index. In the sequel we use this relative frequency histogram to limit such bias as much as possible.
Savitzky-Golay filter (Step 4): The Savitzky-Golay algorithm (polynomial filter) was set with a window of size 11 and a polynomial order of 3 (see scipy.signal.savgol_filter function from the scipy python library).

Peak detection method (Step 5): Peaks were detected as local maxima in the normalized TF distributions. Local maxima were determined according to local conditions. They had a minimal height (h_min = 0.2), a minimal distance from other peaks (d_min = 8), and a minimal prominence (p_min = 0.07). The prominence of a peak measures how much a peak is emerging clearly locally in the signal. It is defined as the vertical distance between the peak and the altitude of the largest region it dominates. These values were found to yield best peak interpretations over the whole set of TFs, in particular to detect multiple peaks in TF distributions such as RunxA. We used the function scipy.signal.find_peaks of the scipy library. In addition to the location of the different peaks p in the signal, the whole range of x values (i.e. the x-axis) is split in intervals [ip,jp] where each peak is prevailing. Cells contributing to peak p can thus only be found in the interval [ip,jp] for each peak p.

Positive cell clusters (Step 5): For each TF, the average number "n" of positive cells was computed in each Lin A/15 iMN observed Cluster corresponding to a detected peak p (using the span [ip,jp] as described above). The procedure varied according to whether only one peak was detected or more than one (multiple peaks can be detected depending on the nature of the data and the parameters defining peaks (see above).

Case of a single detected peak (*e.g.* Jim): The span [ip',jp'] of the active cells under the peak p was computed within the span [ip,jp] by finding the horizontal span under the peak that extends exactly over n cells (green lines on the figures). This cluster [ip',jp'] of positive cells was assumed to correspond to all the cells expressing the TF.

Case of multiple detected peaks (e.g. Nvy (2 peaks) or RunxA (2 peaks)). The sequence was split into the regions [ip,jp] defined by each peak. Then the average number of positive cells "n1", "n2", …, are computed for each of the peak regions. Then the method proceeds within each region and its average number of positive cells as in the case of a single detected peak. This determines both the estimated length and the position of multiple positive cell clusters.

ACKNOWLEDGMENTS

We thank Alain Vincent, Filipe Pinto-Teixeira and Cédric Maurange for comments on the manuscript. We acknowledge the contribution of SFR Biosciences (UAR3444/CNRS, US8/Inserm, ENS de Lyon, UCBL): Arthro-tool facility. We thanks the IGFL microscopy platform. This work was funded by the Atip-Avenir program, FRM (#AJE20170537445) and AFM (#21999) to J.E.

REFERENCES

1. K. M. Allen, S. J. Fung, C. S. Weickert, Cell proliferation is reduced in the hippocampus in schizophrenia. *Aust. N. Z. J. Psychiatry*. **50**, 473–480 (2016).

2. I. Mahar, F. R. Bambico, N. Mechawar, J. N. Nobrega, Stress, serotonin, and hippocampal neurogenesis in relation to depression and antidepressant effects. *Neurosci. Biobehav. Rev.* **38**, 173–192 (2014).

3. H. C. Hazlett, H. Gu, B. C. Munsell, S. H. Kim, M. Styner, J. J. Wolff, J. T. Elison, M. R. Swanson, H. Zhu, K. N. Botteron, D. L. Collins, J. N. Constantino, S. R. Dager, A. M. Estes, A. C. Evans, V. S. Fonov, G. Gerig, P. Kostopoulos, R. C. McKinstry, J. Pandey, S. Paterson, J. R. Pruett, R. T. Schultz, D. W. Shaw, L. Zwaigenbaum, J. Piven, Early brain development in infants at high risk for autism spectrum disorder. *Nature*. **542**, 348–351 (2017).

4. J. Wegiel, I. Kuchna, K. Nowicki, H. Imaki, J. Wegiel, E. Marchi, S. Y. Ma, A. Chauhan, V. Chauhan, T. W. Bobrowicz, M. de Leon, L. A. S. Louis, I. L. Cohen, E. London, W. T. Brown, T. Wisniewski, The neuropathology of autism: defects of neurogenesis and neuronal migration, and dysplastic changes. *Acta Neuropathol. (Berl.)*. **119**, 755–770 (2010).

5. G. Gallardo, Neurogenesis takes a hit in Alzheimer's disease. *Sci. Transl. Med.* **11** (2019), doi:10.1126/scitranslmed.aax1726.

6. S. Jessa, A. Blanchet-Cohen, B. Krug, M. Vladoiu, M. Coutelier, D. Faury, B. Poreau, N. De Jay, S. Hébert, J. Monlong, W. T. Farmer, L. K. Donovan, Y. Hu, M. K. McConechy, F. M. G. Cavalli, L. G. Mikael, B. Ellezam, M. Richer, A. Allaire, A. G. Weil, J. Atkinson, J.-P. Farmer, R. W. R. Dudley, V. Larouche, L. Crevier, S. Albrecht, M. G. Filbin, H. Sartelet, P.-E. Lutz, C. Nagy, G. Turecki, S. Costantino, P. B. Dirks, K. K. Murai, G. Bourque, J. Ragoussis, L. Garzia, M. D. Taylor, N. Jabado, C. L. Kleinman, Stalled developmental programs at the root of pediatric brain tumors. *Nat. Genet.* **51**, 1702–1713 (2019).

7. S. Pop, C.-L. Chen, C. J. Sproston, S. Kondo, P. Ramdya, D. W. Williams, Extensive and diverse patterns of cell death sculpt neural networks in insects. *eLife*. **9**, e59566 (2020).

8. L. L. Prieto-Godino, A. F. Silbering, M. A. Khallaf, S. Cruchet, K. Bojkowska, S. Pradervand, B. S. Hansson, M. Knaden, R. Benton, Functional integration of "undead" neurons in the olfactory system. *Sci. Adv.* **6**, eaaz7238 (2020).

9. K. Harding, K. White, *Drosophila* as a Model for Developmental Biology: Stem Cell-Fate Decisions in the Developing Nervous System. *J. Dev. Biol.* **6** (2018), doi:10.3390/jdb6040025.

10. C. C. Homem, M. Repic, J. A. Knoblich, Proliferation control in neural stem and progenitor cells. *Nat. Rev. Neurosci.* **16**, 647–659 (2015).

11. C. Q. Doe, J. Y. Kuwada, C. S. Goodman, R. L. Gardner, P. A. Lawrence, From epithelium to neuroblasts to neurons: the role of cell interactions and cell lineage during insect neurogenesis. *Philos. Trans. R. Soc. Lond. B Biol. Sci.* **312**, 67–81 (1985).

12. R. Karcavich, C. Q. Doe, *Drosophila* neuroblast 7-3 cell lineage: a model system for studying programmed cell death, Notch/Numb signaling, and sequential specification of ganglion mother cell identity. *J. Comp. Neurol.* **481**, 240–251 (2005).

13. B. C. Bello, N. Izergina, E. Caussinus, H. Reichert, Amplification of neural stem cell proliferation by intermediate progenitor cells in *Drosophila* brain development. *Neural Develop.* **3**, 5 (2008).

14. S. K. Bowman, V. Rolland, J. Betschinger, K. A. Kinsey, G. Emery, J. A. Knoblich, The Tumor Suppressors Brat and Numb Regulate Transit-Amplifying Neuroblast Lineages in *Drosophila*. *Dev. Cell*. **14**, 535–546 (2008).

15. C. C. F. Homem, V. Steinmann, T. R. Burkard, A. Jais, H. Esterbauer, J. A. Knoblich, Ecdysone and Mediator Change Energy Metabolism to Terminate Proliferation in *Drosophila* Neural Stem Cells. *Cell*. **158**, 874–888 (2014).

16. C. Maurange, L. Cheng, A. P. Gould, Temporal Transcription Factors and Their Targets Schedule the End of Neural Proliferation in *Drosophila*. *Cell*. **133**, 891–902 (2008).

17. M. C. Pahl, S. E. Doyle, S. E. Siegrist, E93 Integrates Neuroblast Intrinsic State with Developmental Time to Terminate MB Neurogenesis via Autophagy. *Curr. Biol.* **29**, 750–762.e3 (2019).

18. S. E. Siegrist, N. S. Haque, C.-H. Chen, B. A. Hay, I. K. Hariharan, Inactivation of both Foxo and reaper promotes long-term adult neurogenesis in *Drosophila*. *Curr. Biol. CB*. **20**, 643–648 (2010).

19. C.-P. Yang, T. J. Samuels, Y. Huang, L. Yang, D. Ish-Horowicz, I. Davis, T. Lee, Imp and Syp RNA-binding proteins govern decommissioning of *Drosophila* neural stem cells. *Development*. **144**, 3454–3464 (2017).

20. D. Karlsson, M. Baumgardt, S. Thor, Segment-Specific Neuronal Subtype Specification by the Integration of Anteroposterior and Temporal Cues. *PLOS Biol.* **8**, e1000368 (2010).

21. M. Hailstone, D. Waithe, T. J. Samuels, L. Yang, I. Costello, Y. Arava, E. Robertson, R. M. Parton, I. Davis, CytoCensus, mapping cell identity and division in tissues and organs using machine learning. *eLife*. **9**, e51085 (2020).

22. T. J. Samuels, A. I. Järvelin, D. Ish-Horowicz, I. Davis, Imp/IGF2BP levels modulate individual neural stem cell growth and division through myc mRNA stability. *eLife*. **9**, e51529 (2020).

23. M. Baek, R. S. Mann, Lineage and birth date specify motor neuron targeting and dendritic architecture in adult *Drosophila*. *J. Neurosci. Off. J. Soc. Neurosci.* **29**, 6904–6916 (2009).

24. D. J. Brierley, K. Rathore, K. VijayRaghavan, D. W. Williams, Developmental origins and architecture of *Drosophila* leg motoneurons. *J. Comp. Neurol.* **520**, 1629–1649 (2012).

25. J. Enriquez, L. Q. Rio, R. Blazeski, S. Bellemin, P. Godement, C. Mason, R. S. Mann, Differing Strategies Despite Shared Lineages of Motor Neurons and Glia to Achieve Robust Development of an Adult Neuropil in *Drosophila*. *Neuron*. **97**, 538–554.e5 (2018).

26. W. Guan, S. Bellemin, M. Bouchet, L. Venkatasubramanian, C. Guillermin, A. Laurençon, C. Kabir, A. Darnas, C. Godin, S. Urdy, R. S. Mann, J. Enriquez, Post-transcriptional regulation of transcription factor codes in immature neurons drives neuronal diversity. *Cell Rep.* **39** (2022), doi:10.1016/j.celrep.2022.110992.

27. J. W. Truman, W. Moats, J. Altman, E. C. Marin, D. W. Williams, Role of Notch signaling in establishing the hemilineages of secondary neurons in *Drosophila* melanogaster. *Development*. **137**, 53–61 (2010).

28. T. Awasaki, C.-F. Kao, Y.-J. Lee, C.-P. Yang, Y. Huang, B. D. Pfeiffer, H. Luan, X. Jing, Y.-F. Huang, Y. He, M. D. Schroeder, A. Kuzin, T. Brody, C. T. Zugates, W. F. Odenwald, T. Lee, Making *Drosophila* lineage–restricted drivers via patterned recombination in neuroblasts. *Nat. Neurosci.* **17**, 631–637 (2014).

29. H. Lacin, J. W. Truman, Lineage mapping identifies molecular and architectural similarities between the larval and adult *Drosophila* central nervous system. *eLife*. **5**, e13399 (2016).

30. B. A. Hay, T. Wolff, G. M. Rubin, Expression of baculovirus P35 prevents cell death in *Drosophila*. *Dev. Camb. Engl.* **120**, 2121–2129 (1994).

31. C. Mauvezin, C. Ayala, C. R. Braden, J. Kim, T. P. Neufeld, Assays to monitor autophagy in *Drosophila*. *Methods*. **68**, 134–139 (2014).

32. Z. Liu, C.-P. Yang, K. Sugino, C.-C. Fu, L.-Y. Liu, X. Yao, L. P. Lee, T. Lee, Opposing intrinsic temporal gradients guide neural stem cell production of varied neuronal fates. *Science*. **350**, 317–320 (2015).

33. M. H. Syed, B. Mark, C. Q. Doe, Steroid hormone induction of temporal gene expression in *Drosophila* brain neuroblasts generates neuronal and glial diversity. *eLife*. **6**, e26287 (2017).

34. A. M. Rossi, C. Desplan, Extrinsic activin signaling cooperates with an intrinsic temporal program to increase mushroom body neuronal diversity. *eLife*. **9**, e58880 (2020).

35. J. T. Warren, Y. Yerushalmi, M. J. Shimell, M. B. O'Connor, L. Restifo, L. I. Gilbert, Discrete Pulses of Molting Hormone, 20-Hydroxyecdysone, During Late Larval Development of *Drosophila* melanogaster: Correlations With Changes in Gene Activity. *Dev. Dyn. Off. Publ. Am. Assoc. Anat.* **235**, 315–326 (2006).

36. D. W. Allan, D. Park, S. E. St. Pierre, P. H. Taghert, S. Thor, Regulators Acting in Combinatorial Codes Also Act Independently in Single Differentiating Neurons. *Neuron*. **45**, 689–700 (2005).

37. K. T. Eade, H. A. Fancher, M. S. Ridyard, D. W. Allan, Developmental transcriptional networks are required to maintain neuronal subtype identity in the mature nervous system. *PLoS Genet.* **8**, e1002501 (2012).

38. O. Hobert, Regulation of terminal differentiation programs in the nervous system. *Annu. Rev. Cell Dev. Biol.* **27**, 681–696 (2011).

39. O. Hobert, Terminal Selectors of Neuronal Identity. *Curr. Top. Dev. Biol.* **116**, 455–475 (2016).

40. L.-Y. Liu, X. Long, C.-P. Yang, R. L. Miyares, K. Sugino, R. H. Singer, T. Lee, Mamo decodes hierarchical temporal gradients into terminal neuronal fate. *eLife*. **8** (2019), doi:10.7554/eLife.48056.

41. M. P. J. Dekkers, V. Nikoletopoulou, Y.-A. Barde, Death of developing neurons: New insights and implications for connectivity. *J. Cell Biol.* **203**, 385–393 (2013).

42. R. W. Oppenheim, Cell Death During Development of the Nervous System. *Annu. Rev. Neurosci.* **14**, 453–501 (1991).

43. H.-H. Chen, H.-I. Yu, W.-C. Chiang, Y.-D. Lin, B.-C. Shia, W.-Y. Tarn, hnRNP Q regulates Cdc42-mediated neuronal morphogenesis. *Mol. Cell. Biol.* **32**, 2224–2238 (2012).

44. H. Mori, S. Sakakibara, T. Imai, Y. Nakamura, T. Iijima, A. Suzuki, Y. Yuasa, M. Takeda, H. Okano, Expression of mouse igf2 mRNA-binding protein 3 and its implications for the developing central nervous system. *J. Neurosci. Res.* **64**, 132–143 (2001).

45. K. R. Williams, D. S. McAninch, S. Stefanovic, L. Xing, M. Allen, W. Li, Y. Feng, M. R. Mihailescu, G. J. Bassell, hnRNP-Q1 represses nascent axon growth in cortical neurons by inhibiting Gap-43 mRNA translation. *Mol. Biol. Cell*. **27**, 518–534 (2016).

46. J. Nishino, S. Kim, Y. Zhu, H. Zhu, S. J. Morrison, A network of heterochronic genes including Imp1 regulates temporal changes in stem cell properties. *eLife*. **2**, e00924 (2013).

47. S. C. Lenzken, T. Achsel, M. T. Carrì, S. M. L. Barabino, Neuronal RNA-binding proteins in health and disease. *WIREs RNA*. **5**, 565–576 (2014).

48. N. Degrauwe, M.-L. Suvà, M. Janiszewska, N. Riggi, I. Stamenkovic, IMPs: an RNA-binding protein family that provides a link between stem cell maintenance in normal development and cancer. *Genes Dev.* **30**, 2459–2474 (2016).

49. J. L. Bell, K. Wächter, B. Mühleck, N. Pazaitis, M. Köhn, M. Lederer, S. Hüttelmaier, Insulin-like growth factor 2 mRNA-binding proteins (IGF2BPs): post-transcriptional drivers of cancer progression? *Cell. Mol. Life Sci.* **70**, 2657–2675 (2013).

50. S. Genovese, R. Clément, C. Gaultier, F. Besse, K. Narbonne-Reveau, F. Daian, S. Foppolo, N. M. Luis, C. Maurange, Coopted temporal patterning governs cellular hierarchy, heterogeneity and metabolism in *Drosophila* neuroblast tumors. *eLife*. **8** (2019), doi:10.7554/eLife.50375.

51. Y. Lan, J. Su, Y. Xue, L. Zeng, X. Cheng, L. Zeng, Analysing a Novel RNA-Binding-Protein-Related Prognostic Signature Highly Expressed in Breast Cancer. *J. Healthc. Eng.* **2021**, 9174055 (2021).

52. C. Sun, X. Zheng, Y. Sun, J. Yu, M. Sheng, S. Yan, Q. Zhu, Q. Lan, Identification of IGF2BP3 as an Adverse Prognostic Biomarker of Gliomas. *Front. Genet.* **12**, 743738 (2021).

53. F. Diao, H. Ironfield, H. Luan, F. Diao, W. C. Shropshire, J. Ewer, E. Marr, C. J. Potter, M. Landgraf, B. H. White, Plug-and-Play Genetic Access to *Drosophila* Cell Types using Exchangeable Exon Cassettes. *Cell Rep.* **10**, 1410–1421 (2015).

54. J. B. Skeath, B. A. Wilson, S. E. Romero, M. J. Snee, Y. Zhu, H. Lacin, The extracellular metalloprotease AdamTS-A anchors neural lineages in place within and preserves the architecture of the central nervous system. *Dev. Camb. Engl.* **144**, 3102–3113 (2017).

55. C. T. Rueden, J. Schindelin, M. C. Hiner, B. E. DeZonia, A. E. Walter, E. T. Arena, K. W. Eliceiri, ImageJ2: ImageJ for the next generation of scientific image data. *BMC Bioinformatics*. **18**, 529 (2017).

56. J. Schindelin, I. Arganda-Carreras, E. Frise, V. Kaynig, M. Longair, T. Pietzsch, S. Preibisch, C. Rueden, S. Saalfeld, B. Schmid, J.-Y. Tinevez, D. J. White, V. Hartenstein, K. Eliceiri, P. Tomancak,

A. Cardona, Fiji: an open-source platform for biological-image analysis. *Nat. Methods*. **9**, 676–682 (2012).

57. C. A. Schneider, W. S. Rasband, K. W. Eliceiri, NIH Image to ImageJ: 25 years of image analysis. *Nat. Methods*. **9**, 671–675 (2012).

58. S. Machado, V. Mercier, N. Chiaruttini, LimeSeg: a coarse-grained lipid membrane simulation for 3D image segmentation. *BMC Bioinformatics*. **20**, 2 (2019).

FIGURES and FIGURE LEGENDS

Figure 1. Lin A/15 as model to study how a stereotyped number of neurons is produced by a NB

(A) Drawing of an adult fly showing the position of the CNS (white (cortex), blue (neuropiles)) and Lin A/15 leg MNs (green cell bodies and dendrites in the VNC and axons in the legs). Black box indicates the VNC imaged in **B**. VNC: ventral nerve cord.

(B1) Maximum projection of confocal sections of an adult VNC where the six Lin A/15s are genetically labeled with mCD8::GFP (green). (**B2)** Confocal section of the VNC in **B1** immunostained with anti-Elav (neuronal marker, blue) and anti-Repo (glia marker, yellow). T1, T2 and T3 indicate the Prothoracic, Mesothoracic and Metathoracic neuromere respectively. **(B3-B4)** Confocal section of first left prothoracic neuromere (T1L) (the boxed region in **B2**), arrowheads and arrows indicate Lin A/15 MN and glia cell bodies, respectively. NG: neuropile glia; NP: neuropile; MN: motor neuron.

(C) Drawing of the anterior region of a third instar larva showing the position of the CNS (white (cortex) blue (neuropiles)) and immature LinA/15 leg MNs (green).

(D1) Maximum projection of confocal sections of the second left thoracic hemisegment (T2L) where Lin A/15 is genetically labeled with mCD8::GFP (green). (**D2-D4)** Confocal section of the second left thoracic hemisegment (T2L) in **(D1)** immunostained with anti-Elav (neuronal marker, blue) anti-Dpn (NB marker, cyan) and anti-Repo (glia marker, yellow). Arrowheads, doted arrows and arrows indicate immature Lin A/15 MNs (iMNs), Lin NB and Lin A/15 proliferative glia (PG) respectively. iNP: immature neuropile.

(E1-E2) Plots of the relative position of each Lin A/15 cell from two perspectives: E1 ventral view, E2 lateral view. Axes: Anterior (A), Lateral (L), Ventral (V). Lin A proliferative Glia (PG) are in yellow, Lin A/15 immature MNs (iMNs) are in blue, Lin A/15 GMCs are in white and Lin A/15 NB is in Cyan. Arrows indicate the positions of the confocal sections in (**D2-D4)**.

(F) Graph of the number of Elav+ MNs in a late third instar larva (LL3) vs that in an adult fly.

(G) Schematic of the Lin A/15 type Ib division. NGB: neuroglioblast, NB: neuroblast, IMC: intermediate mother cell, GMC: ganglion mother cell, GB: glioblast, MN: motoneuron. Note 1: the destiny of the MN sister cell during the second phase of division is unknown. Note 2: Lin A/15 development has not been studied during pupal stages.

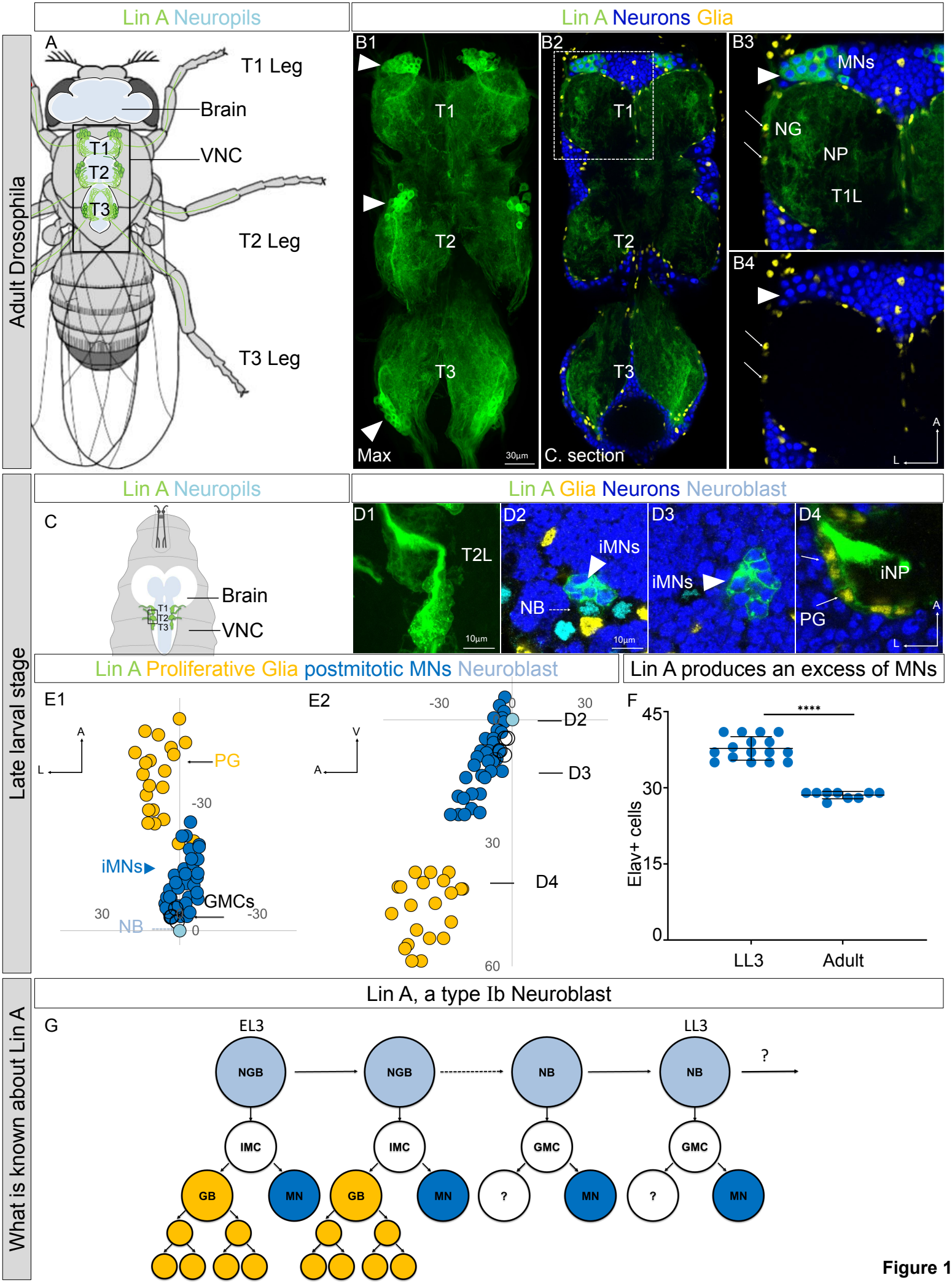
Adult Drosophila
Lin A Neuropils
Lin A Neurons Glia
A
T1 Leg
Brain
VNC
T1
T2
T3
T2 Leg
T3 Leg
B1
T1
T2
T3
Max
30µm
B2
T1
T2
T3
C. section
B3
MNs
NG
NP
T1L
B4
A
L
Late larval stage
Lin A Neuropils
Lin A Glia Neurons Neuroblast
C
Brain
VNC
T1
T2
T3
D1
T2L
10µm
D2
iMNs
NB
10µm
D3
iMNs
D4
iNP
PG
A
L
Lin A Proliferative Glia postmitotic MNs Neuroblast
Lin A produces an excess of MNs
E1
A
L
PG
-30
iMNs
GMCs
30
NB
-30
0
E2
V
A
-30
30
D2
D3
30
D4
60
F
45
30
15
0
Elav+ cells
****
LL3
Adult
What is known about Lin A
Lin A, a type Ib Neuroblast
G
EL3
LL3
NGB
NGB
NB
NB
?
IMC
IMC
GMC
GMC
GB
MN
GB
MN
?
MN
?
MN

Figure 1

Figure 2. The MN sibling cells die through PCD during the second phase of Lin A/15 NB division

(A1-F3) Graphs and confocal images showing the development of Lin A/15 during larval stages, the developmental time points are indicated on top. **(A1, B1, C1, D1, E1, F1)**: Graphs of the relative position of each Lin A/15 cells in **(A3, B3, C3, D3, E3, F3)** from a lateral perspective. Axes: Anterior (A), Ventral (V). Lin A/15 proliferative Glia are in yellow, Lin A/15 immature MNs are in blue, Lin A/15 GMCs are in white, Lin A/15 NB is in Cyan, Lin A/15 cDcp1+ cells are in red. The black lines indicate the positions of the confocal section in (A3-F3). **(A2, B2, C2, D2, E2, F2):** Maximum projection of confocal sections of the second left thoracic hemisegment (T2L) where Lin A/15 is genetically labeled with mCD8::GFP (green). The boxes in **(C2-F2)** are confocal sections showing Lin A/15 NB immunostained with anti-Dpn (cyan). Note: in A2-B2 the NB is easily recognizable by its size (arrowheads). **(A3, B3, C3, D3, E3, F3):** are magnified confocal sections of samples in **(A2, B2, C2, D2, E2, F2)** immunostained with anti- cDcp1(red) , anti-Elav (neuronal marker, blue) and anti-Repo (glia marker, yellow) **(A2, B2)** or with anti-Dpn (NB marker, cyan) **(C2, D2, E2, F2) .** Asterisk in **(B3, C3, D3, E3, F3)** indicate of the cDcp1+ Elav- apoptotic cell.

(G1) Maximum projection of confocal sections of a second right thoracic hemisegment (T2R) with a Lin A/15 MARCM clone genetically labeled with mCD8::GFP (green) under the control of *tub-Gal4* and mCherry (red) under the control of *VGlut-LexA::GAD*. **(G3)** Confocal section of the second right thoracic hemisegment (T2R) (boxed region in G1) immunostained with anti-Elav (blue) and anti-cDcp1 (cyan). The arrowheads indicate the cDcp1+ Elav- *VGlut*- apoptotic cell. **(G2)** Graph of the relative position of each Lin A/15 cell (excluding the proliferative glia) in **(G1)** from a lateral perspective. Axes: Anterior (A), Lateral (L), Ventral (V). Lin A/15 immature MNs are in blue (Elav+), the blue cells surrounded in red are the GFP+ Elav+ Vglut+ immature MNs, the blue cells surrounded in green are the GFP+ Elav+ VGlut- immature MNs (last born MNs) and the cyan cells surrounded in green are the cDcp1+ GFP+ VGlut- Elav- apoptotic cell. Note: the NB (white cell surrounded in green) has been identified by its size. The black line indicates the position of the confocal section in **(G2)**. **(G3)** Confocal section of the second right thoracic hemisegment (T2R) (boxed region in G1) immunostained with anti-Elav (blue) and anti-cDcp1 (cyan). The arrowheads indicate the cDcp1+ Elav- *VGlut*- apoptotic cell.

(H) Schematic of the Lin A/15 type Ib division. NGB: neuroglioblast, NB: neuroblast, IMC: intermediate mother cell, GMC: ganglion mother cell, GB: glioblast, MN: motoneuron. The markers used to label each type of Lin A cells are indicated.

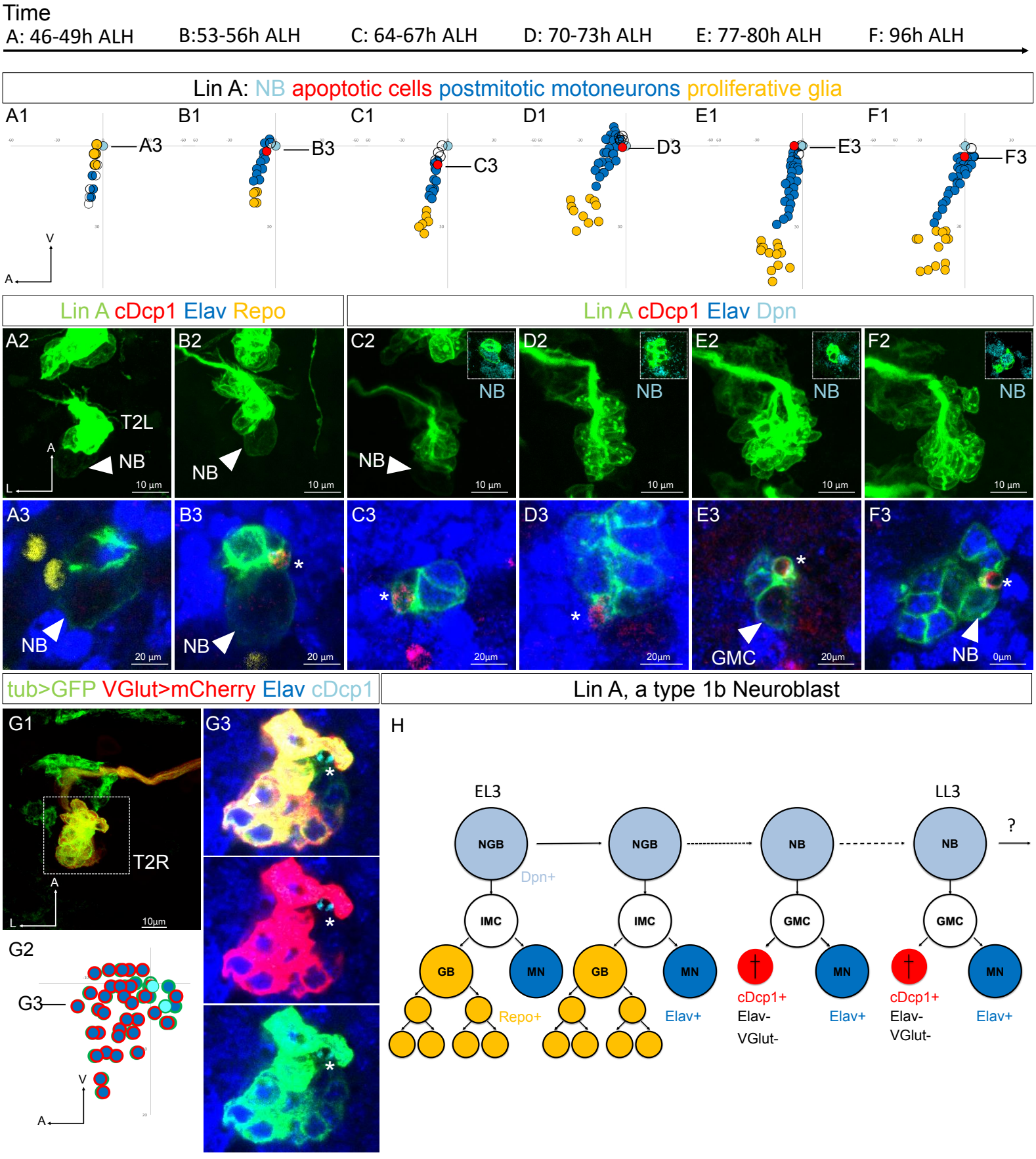
Time
A: 46-49h ALH
B:53-56h ALH
C: 64-67h ALH
D: 70-73h ALH
E: 77-80h ALH
F: 96h ALH
Lin A: NB apoptotic cells postmitotic motoneurons proliferative glia
A1
B1
C1
D1
E1
F1
A3
B3
C3
D3
E3
F3
V
A
Lin A cDcp1 Elav Repo
Lin A cDcp1 Elav Dpn
A2
B2
C2
D2
E2
F2
T2L
NB
10 µm
A3
B3
C3
D3
E3
F3
20 µm
GMC
0µm
tub>GFP VGlut>mCherry Elav cDcp1
Lin A, a type 1b Neuroblast
G1
T2R
10µm
G2
G3
H
EL3
LL3
NGB
Dpn+
IMC
GB
MN
Repo+
Elav+
NB
GMC
cDcp1+
Elav-
VGlut-
?

Figure 2

Figure 3. Lin A/15 NB decommissions at 24h APF through PCD

(A1-C3) Confocal images showing the development of Lin A/15 during pupal stages, the developmental time points are indicated on top. APF: after pupa formation.

(A1, B1, C1) Maximum projection of confocal sections of the first left thoracic hemisegment (T1L) where Lin A/15 is genetically labeled with mCD8::GFP (green). **(A2, B2, C2)** Confocal sections showing Lin A/15 immunostained with anti-Elav (blue), anti-Dpn (cyan) and anti-pH3 (red, phospho-Histone3, mitosis-specific marker **(A3, B3, C3)** magnifications of the boxed region in **(A2, B2, C2)**. Arrowheads indicate the proliferative Lin A/15 NBs (Dpn+ pH3+).

(D1) Maximum projection of confocal sections of three thoracic ganglions (T1, T2, T3) at 24h APF where all 6 Lin A/15s are genetically labeled with mCD8::GFP (green). **(D2)** Confocal section of thoracic ganglions in **(D1)** immunostained with anti-Elav (blue), anti-Dpn (cyan) and anti-cDcp1 (red). **(D2)** magnifications of the boxed region in **(D2)** (left Mesothoracic neuromere, T2L). Arrowheads indicates the apoptotic Lin A/15 NB (Dpn+ cDcp1+).

(E1-F1) Confocal images showing the absence vs presence of Lin A/15 NB at 28h APF in Control vs P35 OE conditions. 6 Lin A/15s are genetically labeled with mCD8::GFP (green), Lin A/15 NB and MNs are visualized with anti-Dpn (red) and anti-Elav (blue) respectively. **(E2-F2)** Magnifications of the boxed region in **(E1-F1)** (first right thoracic hemisegment, T1R) indicate the presence of NB (Dpn+, arrowhead) in P35 OE condition.

(G) Graph of the frequency of NB presence (Number of Lin A/15 samples analyzed is indicated on each bar) at different developmental time points under different genetic conditions: absence of NB (white), NB presence in *Control* (green), NB presence in *P35 OE* (purple).

(H) Schematic of the Lin A/15 type Ib division during larval and pupal stages. NGB: neuroglioblast, NB: neuroblast, IMC: intermediate mother cell, GMC: ganglion mother cell, GB: glioblast, MN: motoneuron. The markers used to label each type of Lin A/15 cells are indicated.

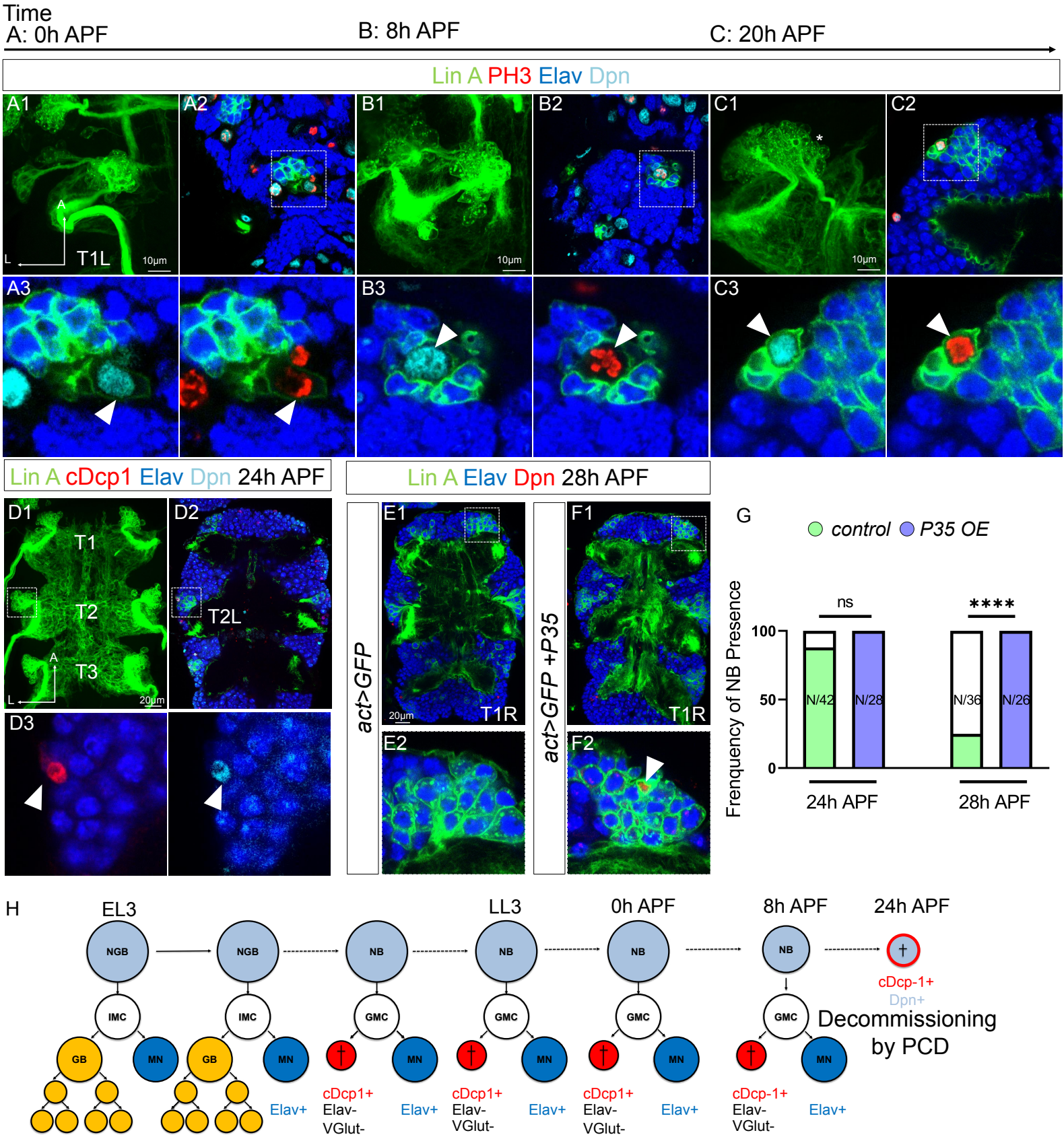
Time
A: 0h APF
B: 8h APF
C: 20h APF
Lin A PH3 Elav Dpn
A1
A2
B1
B2
C1
C2
A3
B3
C3
T1L
10μm
Lin A cDcp1 Elav Dpn 24h APF
Lin A Elav Dpn 28h APF
D1
D2
D3
T1
T2
T3
T2L
20μm
E1
E2
F1
F2
T1R
act>GFP
act>GFP +P35
G
control
P35 OE
Frenquency of NB Presence
ns
****
100
50
0
N/42
N/28
N/36
N/26
24h APF
28h APF
H
EL3
LL3
0h APF
8h APF
24h APF
NGB
NB
IMC
GMC
GB
MN
Elav+
cDcp1+
Elav-
VGlut-
cDcp-1+
Dpn+
Decommissioning
by PCD

Figure 3

Figure 4. Spatio-temporal expression of Imp/Syp in Lin A/15

(A1-J2) Confocal images showing the development of Lin A/15 during larval and pupal stages, the developmental time points are indicated on top. ALH: after larva hatching; APF: after pupa formation. **(A1, B1, C1, D1, E1, F1, G1, H1, I1, J1)** Maximum projection of confocal sections of the second left thoracic hemisegment (T2L) where Lin A/15 is genetically labeled with mCD8::GFP (white). **(A2, B2, C2, D2, E2, F2 G2, H2, I2, J2)** Magnified confocal sections of boxed regions in **(A1, B1, C1, D1, E1, F1, G1, H1, I1, J1)** showing Lin A/15 NB in immunostained with anti-Elav (neuronal marker, blue), anti-Dpn (NB marker, cyan) and anti-Imp (red) **(A2, B2, C2, D2, E2**) or anti-Syp (yellow) **(F2 G2, H2, I2, J2)**. The dashed lines indicates GFP labeled cells including NB and new-born MNs. White arrowheads indicate Lin A/15 NB.

(K) Schematic of the Lin A/15 type Ib division correlating Imp/Syp protein level and spatio-temporal PCD pattern in Lin A/15 cells. NGB: neuroglioblast, NB: neuroblast.

Time
A: 46-49h ALH
B:70-73h ALH
C: 96h ALH
E: 8h APF
F: 23h APF
Lin A Imp, Elav, Dpn
A1
B1
C1
D1
E1
A
L
T2L
5 µm
10µm
A2
B2
C2
D2
E2
NB
Lin A, Syp, Elav, Dpn
F1
G1
H1
I1
J1
F2
G2
H2
I2
J2
K
Imp
Syp
NGB
?
Quiscent NB
IM C
GB
MN #1
MN #2
NB
GM C
MN #29
MN
†
Integration into the connectome
Imp +
Syp +
cDcp1 +
Apoptosis

Figure 4

Figure 5. Opposite temporal expressions of Imp/Syp control the timing of Lin A/15 NB decommissioning

(A1-O2) Confocal images showing the development of *WT* **(A1-C2)**, *Imp RNAi* **(D1-F2)**, from pupal stages until the adult stage.

(A1, B1, C1, D1, E1, F1) Maximum projection of confocal sections of the three right thoracic hemisegments (T1R, T2R, T3R) during pupal stages where Lin A is genetically labeled with mCD8::GFP (green). **(A2, B2, C2, D2, E2, F2)** Confocal sections of boxed regions in **(A1, B1, C1, D1, E1, F1)** immunostained with anti-Elav (neuronal marker, blue) and anti-Dpn (NB marker, cyan). The developmental time points are indicated on the top of each panel. Arrowheads indicate the presence of NB (Dpn+).

(G) Graph of the frequency of NB presence (Number of Lin A/15 samples analysed is indicated on each bar) at different developmental time points under different genetic conditions: absence of NB (white), NB presence in *Control* (green)and NB presence in *Imp RNAi* (orange°.

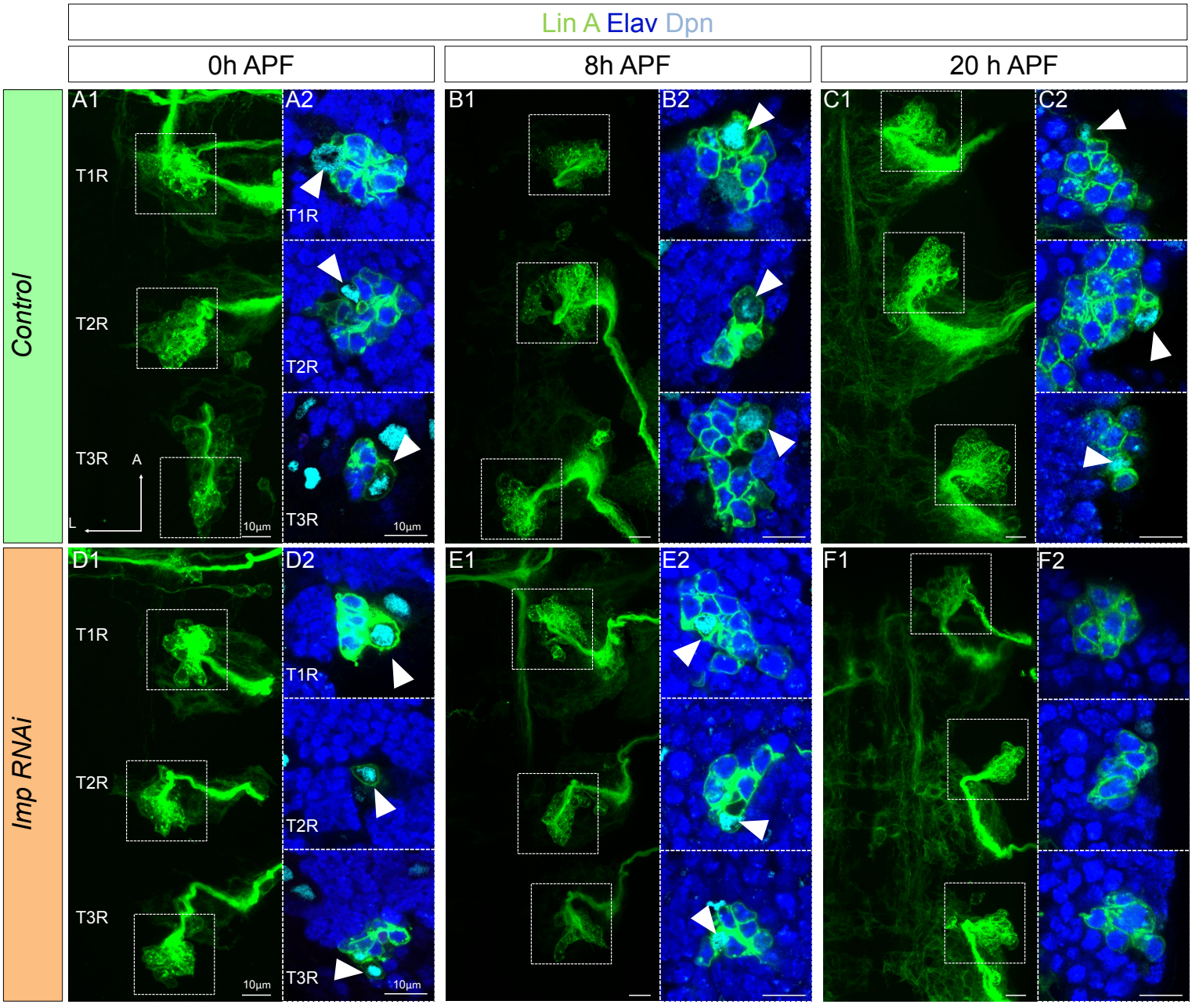
Lin A Elav Dpn
0h APF
8h APF
20 h APF
Control
Imp RNAi
A1
A2
B1
B2
C1
C2
D1
D2
E1
E2
F1
F2
T1R
T2R
T3R
A
L
10μm

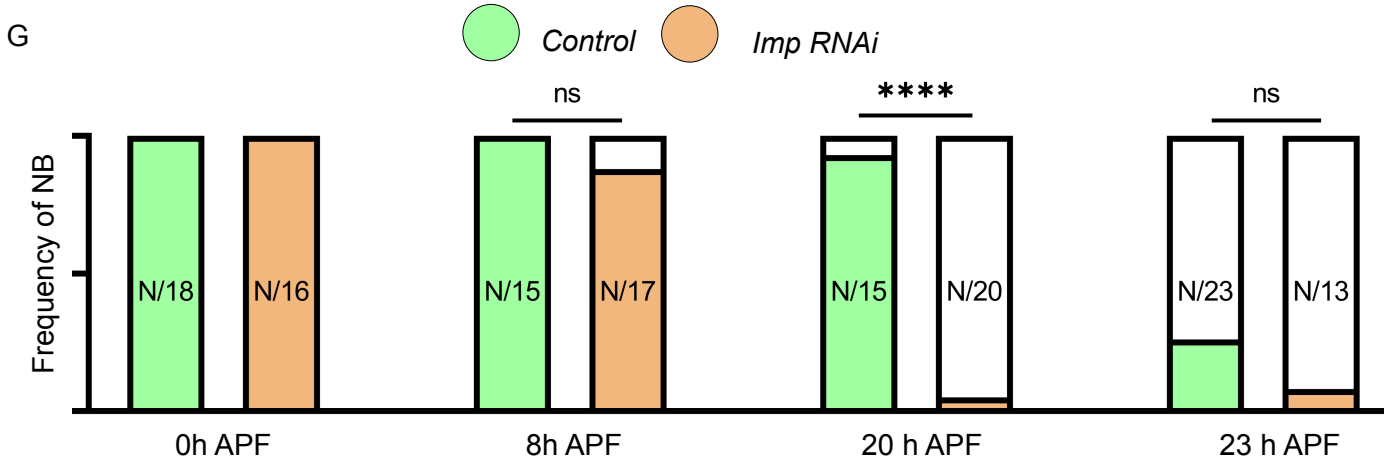
G
Control
Imp RNAi
Frequency of NB
ns
****
ns
N/18
N/16
N/15
N/17
N/15
N/20
N/23
N/13
0h APF
8h APF
20 h APF
23 h APF

Figure 5

Figure 6. Opposite temporal expressions of Imp/Syp control the timing of Lin A/15 NB decommissioning

(A1-I2) Confocal images showing the development of *WT* **(A1-C2)**, *Imp OE* **(D1-F2)** and *Syp RNAi* Lin A/15 **(G1-I2)** from pupal stages until the adult stage.

(A1, B1, C1, D1, E1, F1, G1, H1, I1) Maximum projection of confocal sections of the three right thoracic hemisegments (T1R, T2R, T3R) during pupal stages or in adult VNCs **where** Lin A is genetically labeled with mCD8::GFP (green). **(A2, B2, C2, D2, E2, F2, G2, H2, I2)** Confocal sections of boxed regions in **(A1, B1, C1, D1, E1, F1, G1, H1, I1)** immunostained with anti-Elav (neuronal marker, blue) and anti-Dpn (NB marker, cyan). The developmental time points are indicated on the top of each panel. Arrowheads indicate the presence of NB (Dpn+).

(J) Graph of the frequency of NB presence (Number of Lin A/15 samples analysed is indicated on each bar) at different developmental time points under different genetic conditions: absence of NB (white), NB presence in *Control* (green), NB presence in *Imp RNAi* (orange), NB presence in *Imp OE* (blue) and NB presence in *Syp RNAi* (purple).

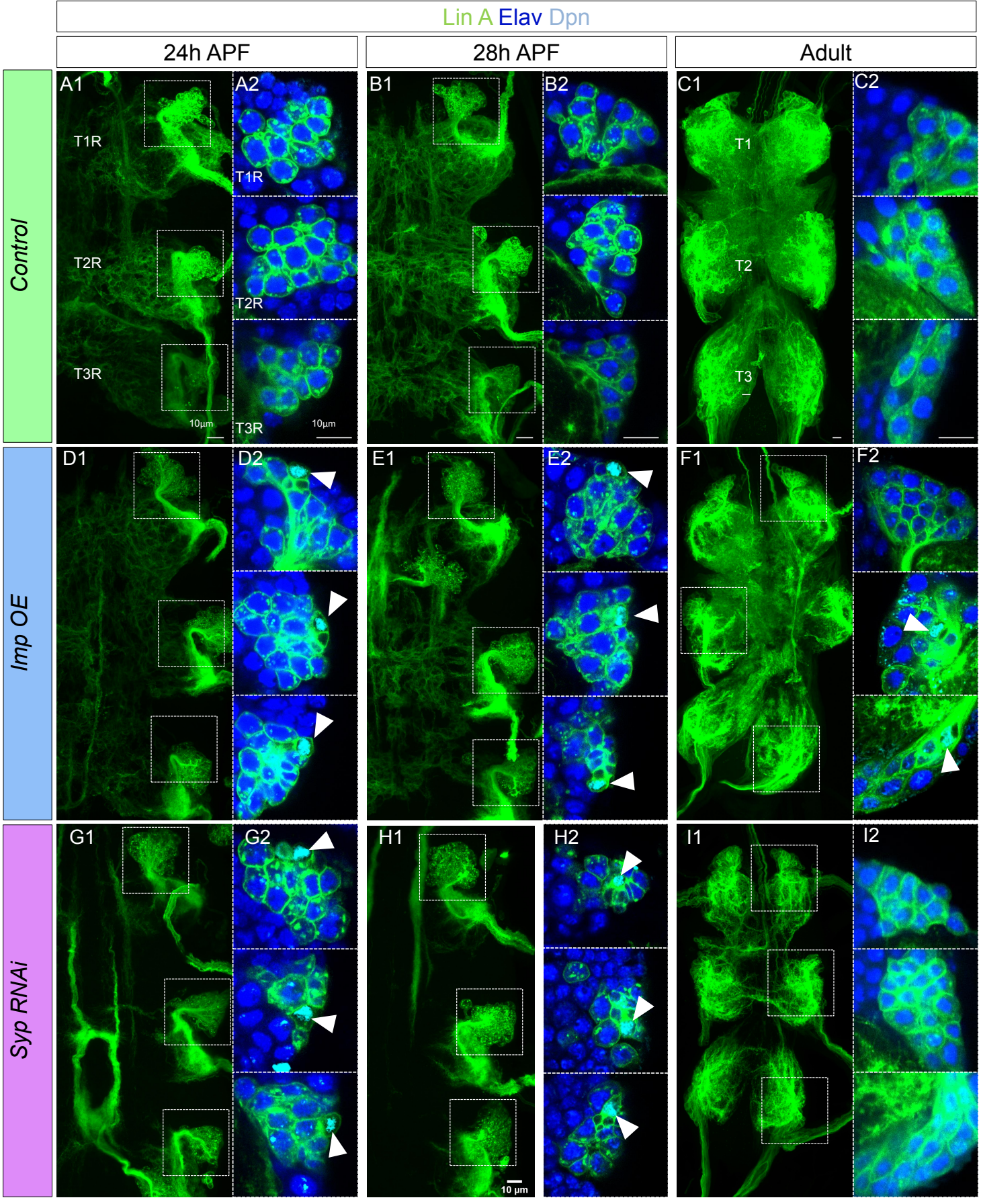
Lin A Elav Dpn
24h APF
28h APF
Adult
Control
Imp OE
Syp RNAi
A1
A2
B1
B2
C1
C2
D1
D2
E1
E2
F1
F2
G1
G2
H1
H2
I1
I2
T1R
T2R
T3R
T1
T2
T3
10μm
10 μm

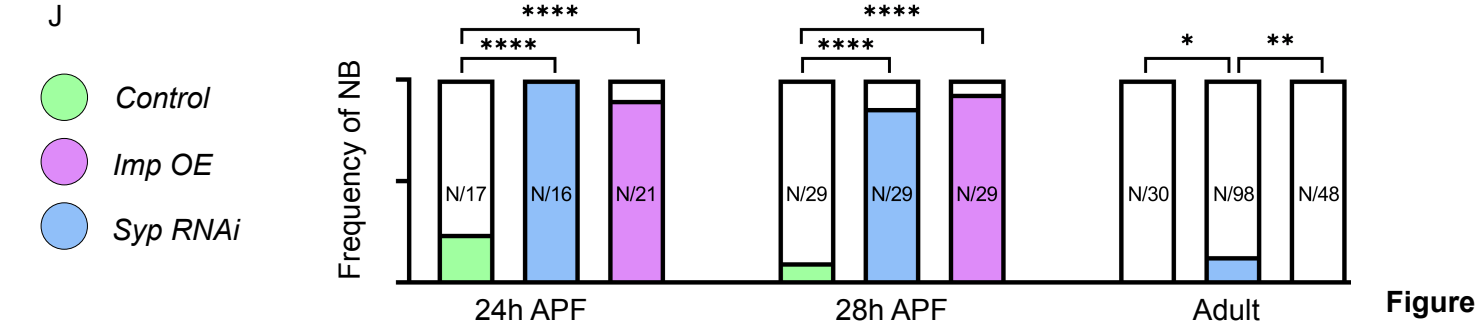
J
Control
Imp OE
Syp RNAi
Frequency of NB
****
****
****
****
*
**
N/17
N/16
N/21
N/29
N/29
N/29
N/30
N/98
N/48
24h APF
28h APF
Adult

Figure 6

Figure 7. The last-born Lin A/15 MNs are eliminated by PCD during early pupal stages.

(A1-C3) Graphs and confocal images showing the PCD pattern in Lin A/15 MNs during pupal stages, the developmental time points are indicated on top.

(A1, B1, C1) Graphs of the relative position of each Lin A/15 cell of the boxed regions in **(A2, B2, C2)** from a lateral perspective. Axes: Anterior (A), Ventral (V). Lin A/15 immature MNs are in blue, Lin A/15 GMCs are in white, Lin A/15 NB is in Cyan and cDcp1+ MNs are in red and blue. The black lines indicate the positions of the confocal sections in **(A3, A4, B3, B4, C3, C4).**

(A2-C3) Confocal sections of Lin A/15 genetically labeled with mCD8::GFP (green). The confocal sections showing the Elav+, cDcp1+ cells immunostained with anti-Dpn (cyan), anti-Elav (blue) and anti-cDcp1 (red) are indicated in **(A1, B1, C1)**. Arrowheads indicate the apoptotic MNs (Elav+, cDcp1+).

(D1) Maximum projection of confocal sections of three left thoracic hemisegments at 5 hour APF where Lin A/15 is genetically labeled with mCD8::GFP (green). **(D2, D3, D4)** Confocal sections of the three left thoracic hemisegments (boxed regions in **(E1)**) immunostained with anti-cDcp1(red), anti-Elav (neuronal marker, blue) and Edu (yellow). Arrowheads indicate the Elav+, cDcp1+ Edu+ cells. Note: the larvae were fed with Edu from 74 to 96 h ALH to label only the last born motoneurons with Edu (close to the NB). The cDcp1+ Elav+ cells are always Edu+. **(D5, D6, D7)** Graphs of the relative position of each Lin A/15 cell of the boxed regions in **(D1)** from a lateral perspective. Axes: Anterior (A), Ventral (V). Lin A/15 immature MNs are in blue, Lin A/15 GMCs are in white, Lin A/15 NB is in Cyan and Elav+, cDcp1+ cells are in red and blue, Edu+ cells are circled in yellow. Note: the last born MNs and the GMCs as well as NB are all Edu+ (circled yellow) and the apoptotic Elav+ cDcp1+ cells is always part of this population of Edu + cells demonstrating that the last born MNs are dying.

(E) Graph of the number of Edu+ Lin A/15 MNs at 5h APF and 17h APF, of which larvae are fed with Edu from 74 to 96 hours ALH. Note: the number of Edu+ cells neurons decrease significantly between 5h and 17h APF demonstrating that the last born MNs are eliminated.

(F) Graph of the number of Elav+ *VGlut*+ Lin A/15 cells in third instar larvae (LL3) and adults (Adult) of *WT* vs *VGlut>P35* Lin A/15 MARCM clones.

(G-J) Maximum projection of confocal sections of the left T1 segment (T1L) of third instar larva **(G-H)** and the left prothoracic neuromere (T1L) in adult fly **(I-J)** containing a WT **(G, I)** or a *VGlut>P35* **(H,J)** Lin A/15 MARCM clone. The boxed regions inserted in each picture in **(G-J)** indicate the Elav+ GFP+ cells.

(L) Graph of the number of Elav+ Lin A/15 neurons at different developmental time points.

(M) Schematic of the Lin A/15 type Ib division during larval and pupal stages. NGB: neuroglioblast, NB: neuroblast, IMC: intermediate mother cell, GMC: ganglion mother cell, GB: Glioblast, MN: motoneuron.

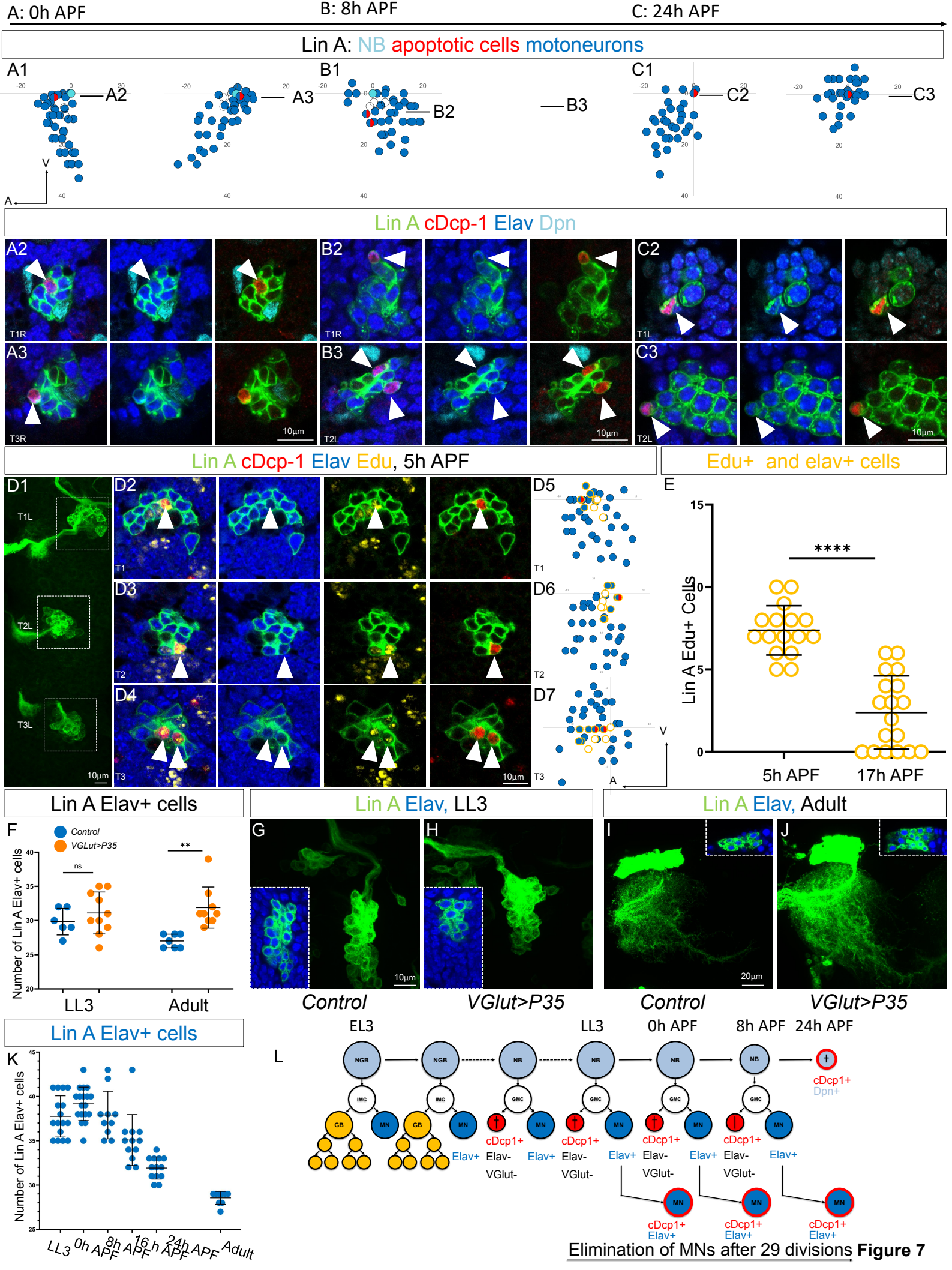
A: 0h APF
B: 8h APF
C: 24h APF
Lin A: NB apoptotic cells motoneurons
A1
A2
A3
B1
B2
B3
C1
C2
C3
V
A
Lin A cDcp-1 Elav Dpn
T1R
T3R
T2L
T1L
10µm
Lin A cDcp-1 Elav Edu, 5h APF
D1
D2
D3
D4
D5
D6
D7
T1
T2
T3
T1L
T2L
T3L
Edu+ and elav+ cells
E
Lin A Edu+ Cells
****
5h APF
17h APF
Lin A Elav+ cells
F
Control
VGLut>P35
ns
**
Number of Lin A Elav+ cells
LL3
Adult
Lin A Elav, LL3
Lin A Elav, Adult
G
H
I
J
20µm
Control
VGlut>P35
Lin A Elav+ cells
K
LL3
0h APF
8h APF
16 h APF
24h APF
Adult
L
EL3
LL3
0h APF
8h APF
24h APF
NGB
NB
IMC
GMC
GB
MN
cDcp1+
Dpn+
Elav+
Elav-
VGlut-
Elimination of MNs after 29 divisions

Figure 7

Figure 8. The opposite expression pattern in immature neurons of Imp/Syp instructs the number of surviving MN

(A1) Maximum projection of confocal sections of the T1R hemisegment where Lin A/15 is genetically labeled with mCD8::GFP (green) at 5h APF. **(A2, A3, A4, A5)** are confocal sections of the Lin A/15 in **(A1)** showing the apoptotic MN immunostained with anti-Imp (red), anti-Elav (blue) and anti-cDcp1 (cyan) of **(A1)**. Arrowheads indicate the apoptotic MN (Elav+, cDcp1+) is absent of Imp (Imp-).

(B1-B2) Graph of the number of apoptotic MNs (Elav+, cDcp1+) observed in Lin A/15 at different developmental time points under different genetic conditions: *Control* (green) , *Imp RNAi* (orange)*, Imp OE* (blue) and *Syp RNAi* (purple).

(C1, D1, E1, F1, G1, H1, I1, J1) Maximum projection of confocal sections of the second right thoracic hemi-segments (T2R) where Lin A/15 is genetically labeled with mCD8::GFP (green) under different genetic conditions *control* **(C1, E1, H1)**, *Imp RNAi* **(D1)***, Imp OE* **(F1, I1,)** and *Syp RNAi* **(G1, J1)**. **(C2, D2, E2, F2, G2, H2, I2, J2)** Confocal sections of the second right thoracic hemisegment (T2R) in **(C1, D1, E1, F1, G1, H1, I1, J1)** immunostained with anti- cDcp1(red), anti-Elav (neuronal marker, blue and anti-Dpn (NB marker, cyan). The boxed region in **(D2, E2, H2, J2)** indicated the presence of Elav+ cDcp1+ cells. **(C3, D3, E3, F3, G3, H3, I3, J3)** Graphs of the relative position of each Lin A/15 cell in **(C1, D1, E1, F1, G1, H1, I1, J1)** from a lateral perspective. Axes: Anterior (A), Ventral (V). Lin A/15 immature MNs are in blue, Lin A/15 GMCs are in white, Lin A/15 NB is in Cyan and cDcp1+ Elav+ neurons are in red and blue.

(K) Graph of the number of Elav+ Lin A/15 neurons observed in adult flies under different genetic conditions: *control* (green), *Imp RNAi* (orange)*, Imp OE* (blue) and *Syp RNAi* (purple).

(L1-M1) Maximum projection of confocal sections of the left prothoracic neuromere (T1L) containing a control **(L1)** or a *VGlut>Imp* **(M1)** Lin A/15 MARCM clone. The boxed regions in **(L1-M1)** are confocal sections showing the Lin A/15 Elav+ (anti-Elav, Blue) GFP+ cells. **(L2-M2)** Graphs of the relative position of each Lin A/15 cell in **(L1, M1)** from a lateral perspective. Axes: Anterior (A), Ventral (V). Lin A/15 immature MNs are in blue.

(N) Graph of the number of Elav+ *VGlut*+ Lin A/15 cells of control and *VGlut>Imp* Lin A/15 MARCM clones in third instar larvae (LL3) and adult flies.

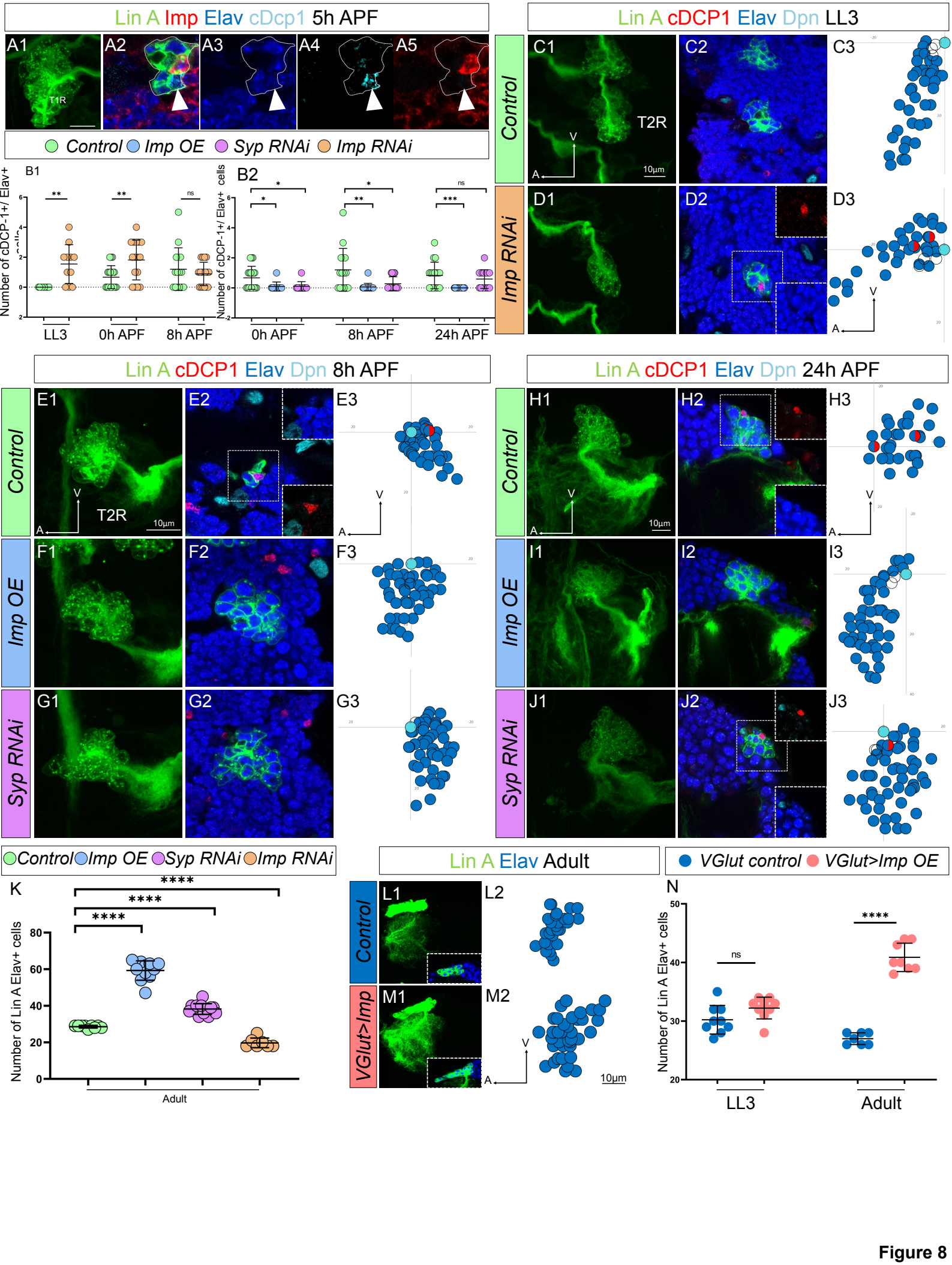
Lin A Imp Elav cDcp1 5h APF
A1
T1R
A2
A3
A4
A5
Control Imp OE Syp RNAi Imp RNAi
B1
B2
Number of cDCP-1+/ Elav+ cells
LL3
0h APF
8h APF
0h APF
8h APF
24h APF
Lin A cDCP1 Elav Dpn LL3
Control
Imp RNAi
C1
T2R
C2
C3
D1
D2
D3
Lin A cDCP1 Elav Dpn 8h APF
E1
T2R
10µm
E2
E3
F1
F2
F3
G1
G2
G3
Lin A cDCP1 Elav Dpn 24h APF
H1
H2
H3
I1
I2
I3
J1
J2
J3
Control
Imp OE
Syp RNAi
Control Imp OE Syp RNAi Imp RNAi
K
Number of Lin A Elav+ cells
Adult
Lin A Elav Adult
L1
L2
M1
M2
VGlut>Imp
VGlut control VGlut>Imp OE
N
Number of Lin A Elav+ cells
ns
LL3
Adult

Figure 8

Figure 9. The last-born MNs eliminated by PCD are primed with a specific combination of TFs under control of Imp and Syp.

(A1, B1, C1, E1, F1, G1, I1, J1, K1) Plots of the relative position of each Lin A/15 cell from a lateral perspectives showing the expression of Jim **(A1, B1, C1,)**, RunXA **(E1, F1, G1)**, and Nvy **(I1, J1, K1)** in purple**,** orange and green respectively, the Elav+ MNs (blue), the NB (cyan) and the GMC in control **(A1, E1, I1,)**, Imp OE **(B1, F1, J1)** and Syp RNAi **(C1, G1, K1)**.

(A2-A3, B2-B3, C2-C3, E2-E3, F2-F3, G2-G3, I2-I3, J2-J3, K2-K3) confocal sections showing the expression of Jim **(A2-A3, B2-B3, C2-C3,)**, RunXA **(E2-E3, F2-F3, G2-G3,)**, and Nvy **(I2-I3, J2-J3, K2-K3)** in RED, the Elav+ MNs (blue), the Dpn+ NB (cyan). The position of the sections are shown in **(A1, B1, C1, E1, F1, G1, I1, J1, K1).** The asterisk indicate the NBs. Note 1: The arrowhead in B2 indicates a jim+ neurons close to NB, this is never seen in the control LinA/15. Note 2: The arrowheads in E2 indicate RunXA+ neurons close to NB, this is never seen in ImpOE and Syp RNAi LinA/15. Note3: the arrowheads in I2, J2 and K2 indicate NVy + neurons close to the NB, the expression of Nvy is barely detectable in ImpOE and Syp RNAi LinA/15.

(A4, B4, C4, E4, F4, G4, I4, J4, K4) Graphs of the frequency of Jim **(A4, B4, C4)** , RunXA (**E4, F4, (G4,)** and Nvy **(I4, J4, K4)** expression as a function of x' (x': MN ordering axis according to their relative distance from the NB among >15 specimens before (gray bare) and after (colored lines) applying a Savitzky-Golay filter (see material and methods) in control **(A4, E4, I4)**, Imp OE **(B4, F4, J4)** and Syp RNAi **(C4, G1, K4)**. The horizontal bar indicates the Jim+ cell cluster detected with the PCCD method.

(D1-D2, H1-H2, L1-L2) Graphs of the number of Elav+ Lin A/15 MNs **(D1, H1 and L1)** and graphs of the number of Elav+ Lin A/15 MNs expressing Jim **(D2)** , RunXA (**H2)** and Nvy **(L2)** in control, Imp OE and Syp RNAi LinA/15.

(M) Schematic of the TF codes expressed in each iMN predicted by the PCCD method in an L3 larva in control, Imp OE and Syp RNAi LinA/15). Bottom: schematic of the cell body of Lin A/15 iMNs. The numbers inside indicate their relative distances from NB. Top: the horizontal bars indicate the TF+ cell clusters detected with the PCCD method. The dotted lines indicate the coverage index at the border (see material and methods).

Note 1: The arrowheads in B2 indicate a Jim+ neurons

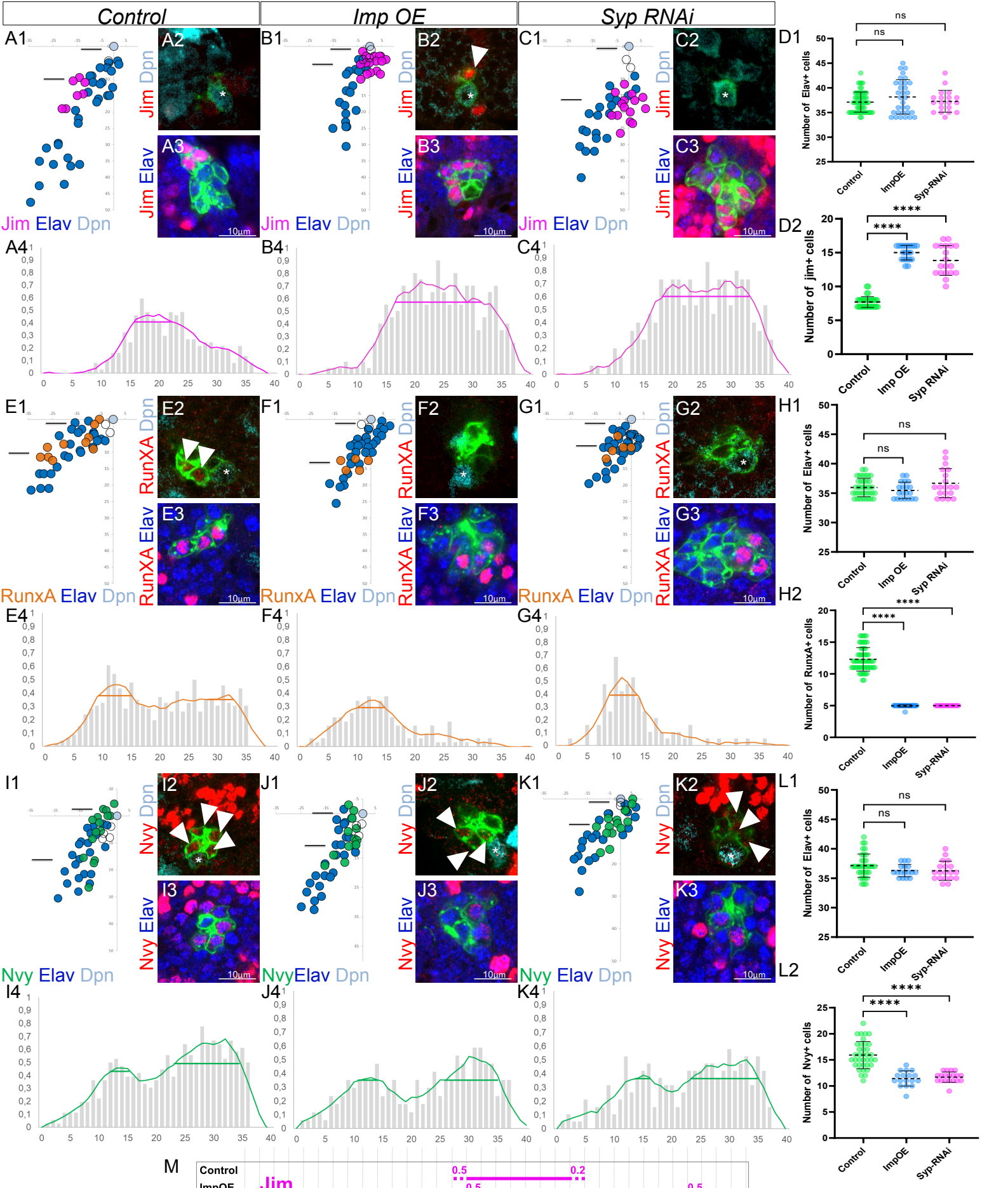
Control
Imp OE
Syp RNAi
A1
A2
A3
B1
B2
B3
C1
C2
C3
D1
Jim Elav Dpn
Jim Dpn
Jim Elav
10µm
ns
Number of Elav+ cells
Control
ImpOE
Syp-RNAi
A4
B4
C4
D2
****
Number of jim+ cells
Imp OE
Syp RNAi
E1
E2
E3
F1
F2
F3
G1
G2
G3
H1
RunxA Elav Dpn
RunXA Dpn
RunXA Elav
Number of Elav+ cells
E4
F4
G4
H2
Number of RunxA+ cells
I1
I2
I3
J1
J2
J3
K1
K2
K3
L1
Nvy Elav Dpn
Nvy Dpn
Nvy Elav
Number of Elav+ cells
I4
J4
K4
L2
Number of Nvy+ cells
M
Control
ImpOE
Syp RNAi
Jim
RunxA
Nvy
0.5
0.2
0.8
0.3
0.7
0.1
0.9
0.6
0.4
1 2 3 4 5 6 7 8 9 10 11 12 13 14 15 16 17 18 19 20 21 22 23 24 25 26 27 28 29 30 31 32 33 34

Figure 9

Figure 10. Changing the combination of TF in last-born MNs leads to MN survival.

(A1-D3) Maximum projection of confocal sections of a right prothoracic hemisegment (T2R) with a Lin A/15 MARCM clone genetically labeled with mCD8::GFP (green) under the control of *VGlut-Gal4* **(A1, B1, C1, D1)** and confocal sections trough LinA/15 (green) and labeled with Elav (red) (**A2-A3, B2-B3, C2-C3, D2-D3)** in different genetic conditions: control **(A2-A3),** *nvy-/-* **(B2-B3)**, *UAS-jim* **(C2-C3),** *nvy-/-*; *UAS-jim* **(D2-D3).**

(E) Graphs of the number of Elav+ VGlut+ MNs in control **,** *nvy-/-* **(B2-B3),** *UAS-Jim* **(C2-C3),** *nvy-/-*; *UAS-jim* **(D2-D3)** MARCM clones.

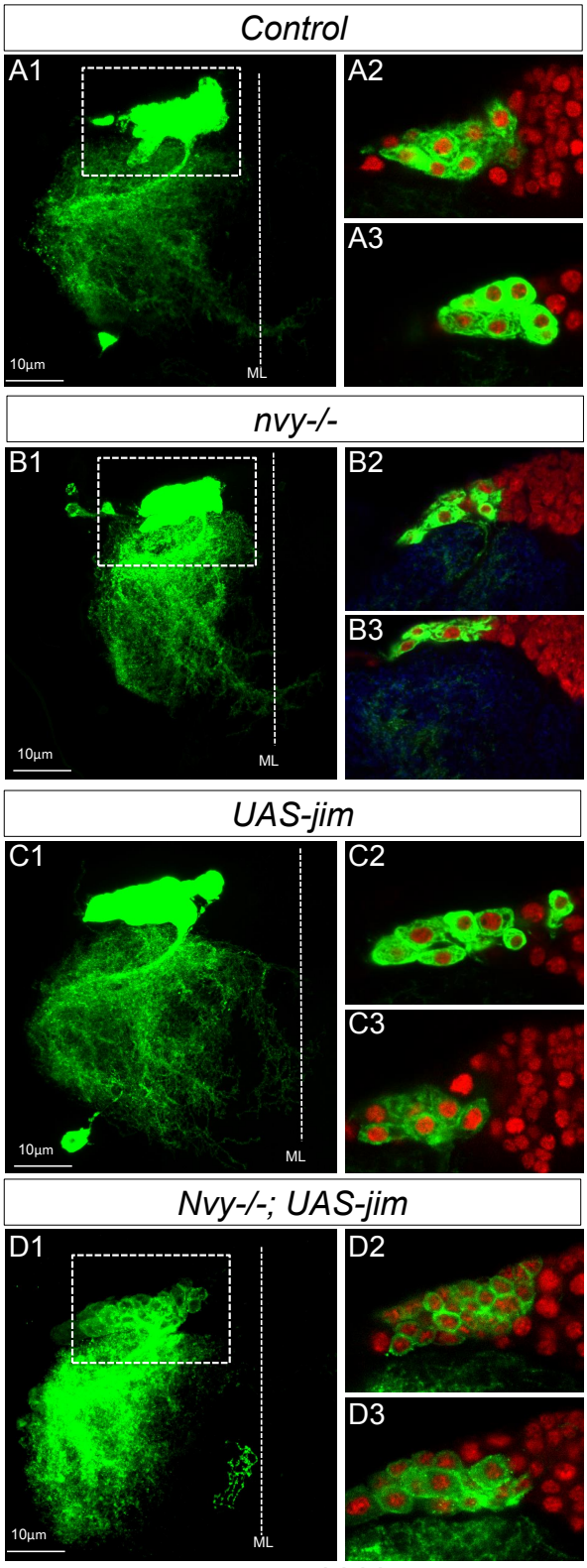
Control
A1
A2
A3
10µm
ML
nvy-/-
B1
B2
B3
10µm
ML
UAS-jim
C1
C2
C3
10µm
ML
Nvy-/-; UAS-jim
D1
D2
D3
10µm
ML

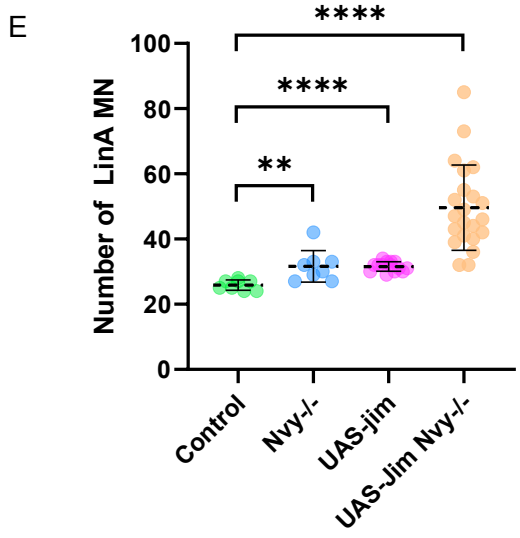
E
****
****
**
Number of LinA MN
100
80
60
40
20
0
Control
Nvy-/-
UAS-jim
UAS-Jim Nvy-/-

Figure 10

Figure S1. The MN sibling cells die through PCD during the second phase of Lin A/15 NB division

(A1-C2) Lin A/15 during pupal stages: 0 hour APF **(A1-A2)**, 8 hours APF **(B1-B2)**, 24 hours APF **(C1-C2). (A2, B2, C2):** Maximum projection of confocal sections of the third left (T3L) **(A1)**, first right (T1R) **(B1)** and second right (T2R) **(C1)** thoracic hemisegments where Lin A/15 is genetically labeled with mCD8::GFP (green). **(A2, B2, C2):** Confocal sections of the corresponding Lin A/15 in **(A1, B1, C1)** immunostained with anti-cDcp1 (red) , anti-Elav (neuronal marker, blue) and anti-Dpn (NB marker, cyan), boxed region showing the dying sibling cells (Elav-, cDcp1+), indicated with arrowheads.

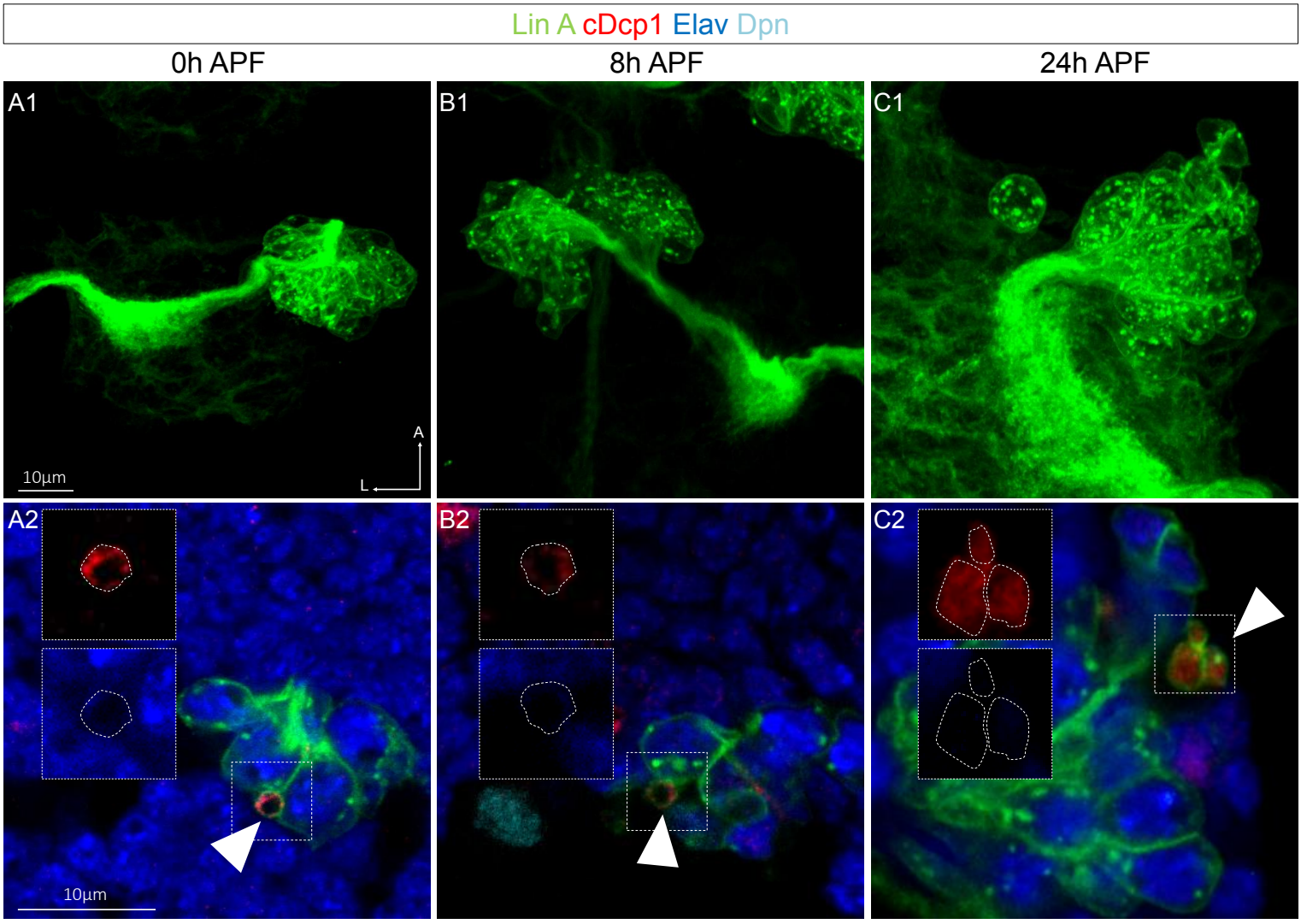
Lin A cDcp1 Elav Dpn
0h APF
8h APF
24h APF
A1
B1
C1
A
L
10µm
A2
B2
C2
10µm

Figure S1

Figure S2. The volume of the Lin A/15 NB continuously decrease during development.

(A) Graph of the volume of the Lin A/15 NB at different time point. X axis: different time points during larval and pupal stages, Y axis: volume of the NB in nano^{m3}.

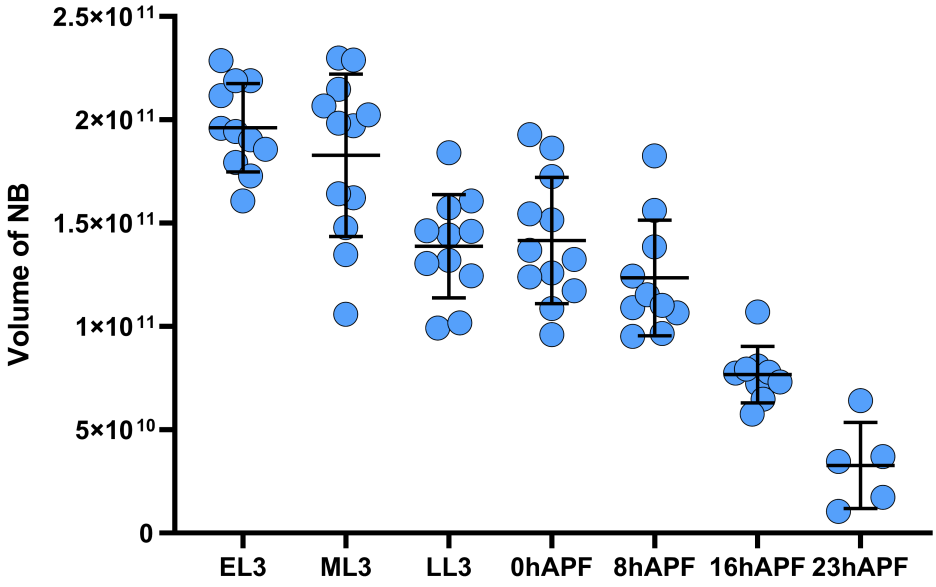
2.5×10 11
2×10 11
1.5×10 11
1×10 11
5×10 10
0
Volume of NB
EL3
ML3
LL3
0hAPF
8hAPF
16hAPF
23hAPF

Figure S2

Figure S3. Lin A/15 NB does not enter into autophagy.

(A1-B3) Lin A/15 during pupal stages: 17 hours APF **(A1-A3)**, 20 hours APF **(B1-B3)**. **(A1, B1)** Maximum projection of confocal sections of the first two thoracic hemisegments where Lin A/15 is genetically labeled with mCherry (red). **(A2-A3, B2-B3):** Confocal sections of the boxed regions in (**A1, B1)** corresponding to the second right thoracic hemisegment (T2R)**.** Lin A/15 is inmunostained with anti-Elav (neuronal marker, blue) and anti-Dpn (NB marker, cyan) and genetically labeled with Atg8::GFP . Arrowheads indicate the NBs.

(C1-C3) Lin A/15 at 23 hours APF. **(C1)** Maximum projection of confocal sections of the first two thoracic hemisegments where Lin A/15 is genetically labeled with GFP (green). **(C1-C3):** Confocal sections of the boxed regions in (**C1)** corresponding to the second right thoracic hemisegment (T2R)**.** Lin A/15 is immunostained with anti-Elav (neuronal marker, blue) and anti-Dpn (NB marker, cyan) and labeled with Lysotracker. Arrowheads indicate the NBs.

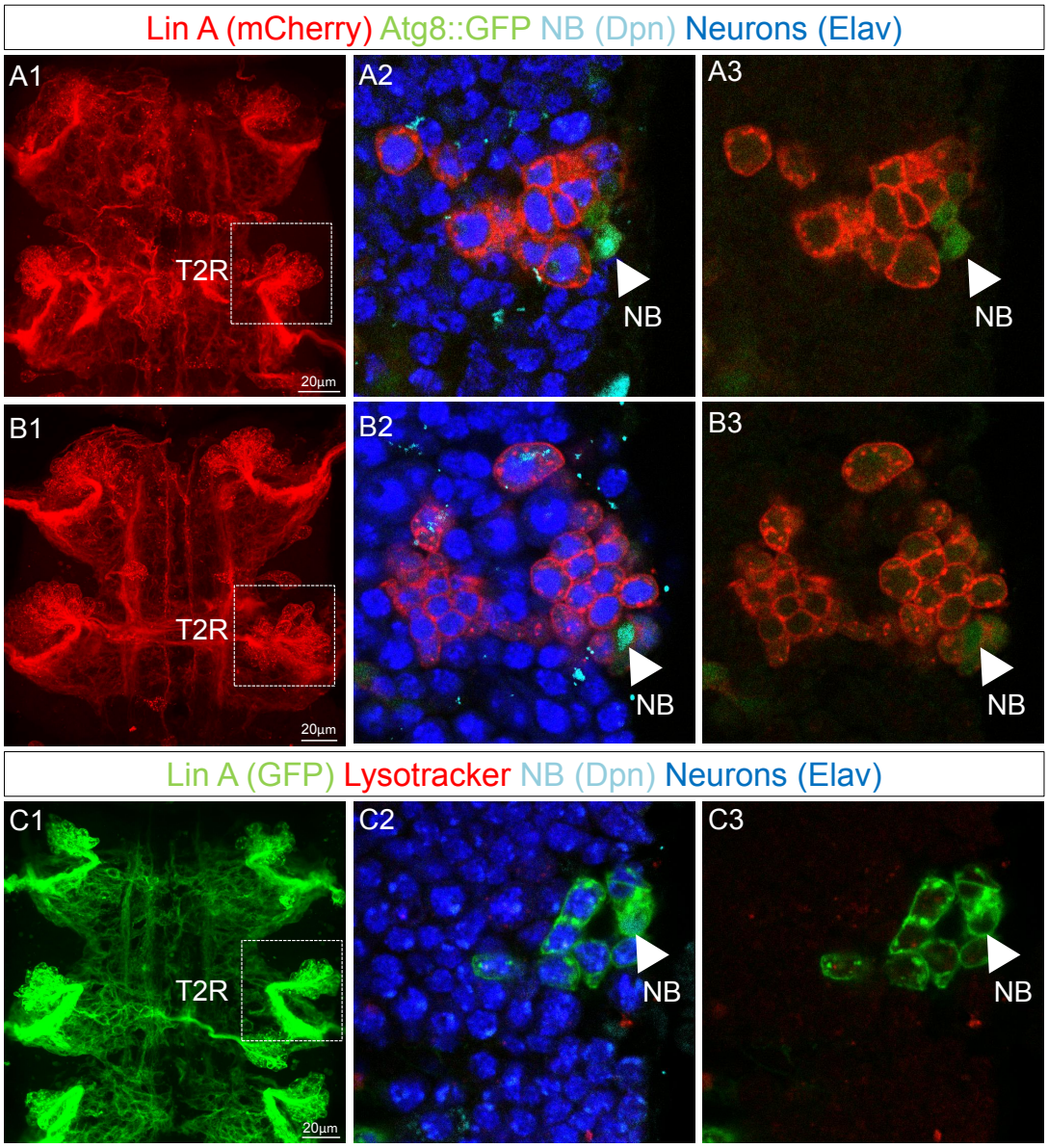
Lin A (mCherry) Atg8::GFP NB (Dpn) Neurons (Elav)
17h APF
20h APF
A1
A2
A3
B1
B2
B3
T2R
NB
20µm

Lin A (GFP) Lysotracker NB (Dpn) Neurons (Elav)
23h APF
C1
C2
C3
T2R
NB
20µm

Figure S3

Figure S4. Syp OE d not change the number of Mns produced by Lin A.

(A-B) Maximum projection of confocal sections of the prothoracic segments with one (A) wt or two syp OE (B) Lin A/15 MARCM clones (mcherry, red) labeled with Elav (green). Graph of the number of Elav+ VGlut+ Lin A MNs in control and Syp OE MARCM clones.


Elav Lin A Adult
A
control
20µm
B
Syp OE
C
Number of LinA MN
40
35
30
25
20
ns
Control
Syp OE

Figure S4

Figure S5. No mutual inhibition between Imp and Syp in Lin A/15.

(A1-D3) Graphs and confocal images showing Syp level at 94-97 AEL in Imp RNAi **(A1-B3)** and Imp level at 120 AEL in Syp RNAi **(C1-D3),** AEL: after egg laying. **(A1, B1, C1, D1)** Graphs of the relative position of each Lin A/15 cells of samples in **(A2-D2)** from a lateral perspective. Axes: Anterior (A), Ventral (V). The black lines indicate the positions of the confocal section in **(A3-D3)**. **(A2, B2, C2, D2)** Confocal sections comparing Syp expression in Lin A/15 NB between WT **(A2)** and Imp RNAi **(B2)**; Imp expression in Lin A/15 NB between control **(C2)** and Syp RNAi **(D2).** Stainings: anti-Dpn (NB marker, cyan) and anti-Imp (red) and anti-Syp (yellow). Boxed regions highlight Imp expression in Nbarrowheads indicated Lin A/15 NB, dashed lines indicate GFP labeled NB. **(A3, B3, C3, D3)** Confocal sections comparing Syp expression in Lin A/15 progenies between control **(A3)** and Imp RNAi **(B3)**; Imp expression in Lin A/15 progenies between control **(C3)** and Syp RNAi **(D3).** Boxed regions highlight Syp expression in MNarrowheads indicated Lin A/15 progenies, dashed lines indicates GFP labeled cells. **(E)** Graph showing the number of Lin A/15 cells (left panels in each graph) and number of Syp/Imp-expressing Lin A/15 progenies (right panel in each graph) in indicated genetic backgrounds.

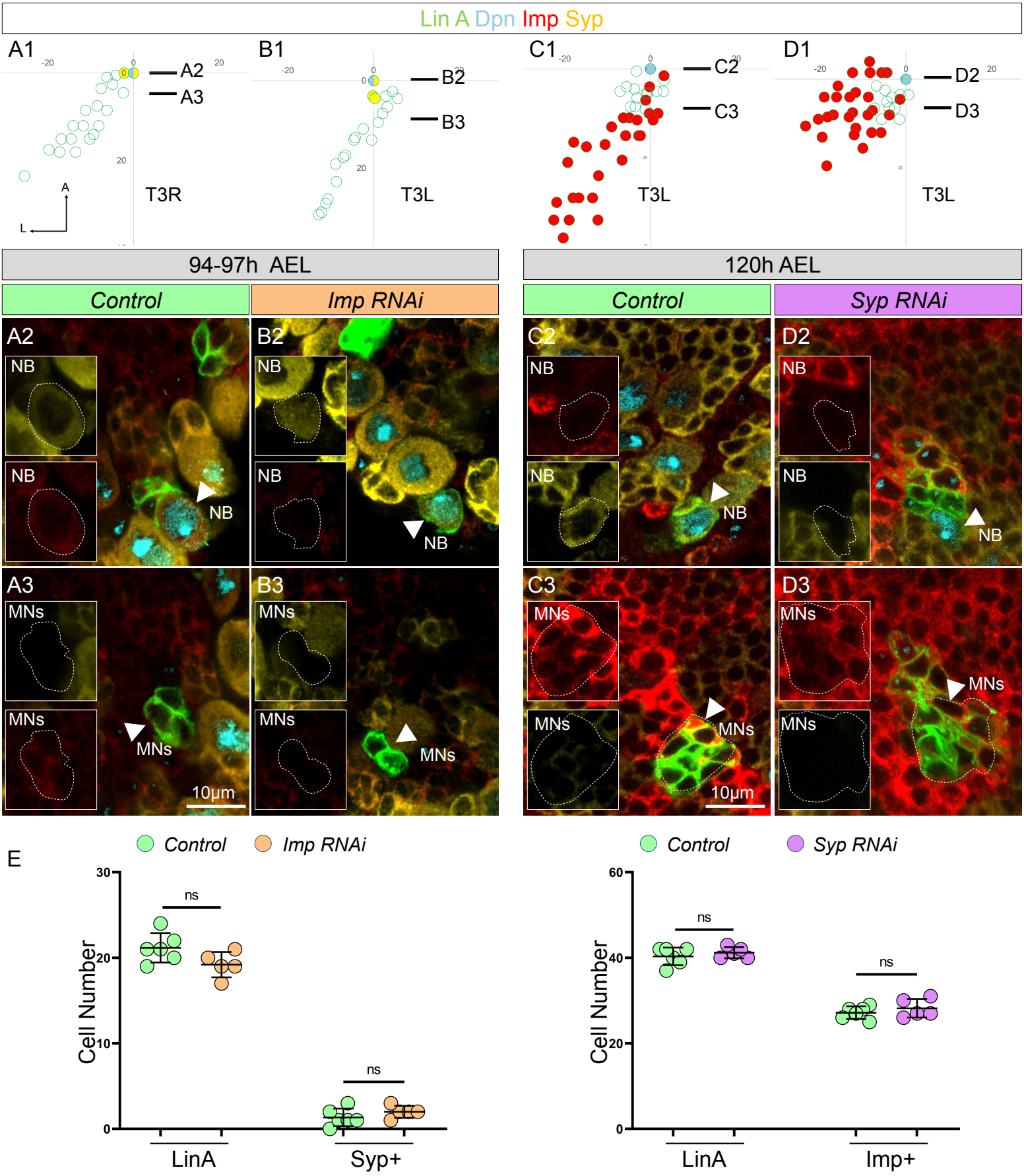
Lin A Dpn Imp Syp
A1
A2
A3
T3R
B1
B2
B3
T3L
C1
C2
C3
T3L
D1
D2
D3
T3L
94-97h AEL
120h AEL
Control
Imp RNAi
Control
Syp RNAi
NB
MNs
10μm
E
Control
Imp RNAi
Cell Number
ns
LinA
Syp+
Control
Syp RNAi
Cell Number
ns
LinA
Imp+

Figure S5